Future Change of North Atlantic Tropical Cyclone Tracks: Projection by a 20-km-Mesh Global Atmospheric Model*

HIROYUKI MURAKAMI+

Advanced Earth Science and Technology Organization, Meteorological Research Institute, Tsukuba, Japan

BIN WANG

Department of Meteorology, and International Pacific Research Center, University of Hawaii at Manoa, Honolulu, Hawaii

(Manuscript received 9 July 2009, in final form 23 November 2009)

ABSTRACT

Possible future change in tropical cyclone (TC) activity over the North Atlantic (NA) was investigated by comparison of 25-yr simulations of the present-day climate and future change under the A1B emission scenario using a 20-km-mesh Meteorological Research Institute (MRI) and Japan Meteorological Agency (JMA) atmospheric general circulation model. The present-day simulation reproduces many essential features of observed climatology and interannual variability in TC frequency of occurrence and tracks over the NA. For the future projection, the model is driven by the sea surface temperature (SST) that includes a trend projected by the most recent Intergovernmental Panel on Climate Change (IPCC) multimodel ensemble and a year-to-year variation derived from the present-day climate. A major finding is that the future change of total TC counts in the NA is statistically insignificant, but the frequency of TC occurrence will decrease in the tropical western NA (WNA) and increase in the tropical eastern NA (ENA) and northwestern NA (NWNA). The projected change in TC tracks suggests a reduced probability of TC landfall over the southeastern United States, and an increased influence of TCs on the northeastern United States. The track changes are not due to changes of large-scale steering flows; instead, they are due to changes in TC genesis locations. The increase in TC genesis in the ENA arises from increasing background ascending motion and convective available potential energy. In contrast, the reduced TC genesis in the WNA is attributed to decreases in midtropospheric relative humidity and ascending motion caused by remotely forced anomalous descent. This finding indicates that the impact of remote dynamical forcing is greater than that of local thermodynamical forcing in the WNA. The increased frequency of TC occurrence in the NWNA is attributed to reduced vertical wind shear and the pronounced local warming of the ocean surface. These TC changes appear to be most sensitive to future change in the spatial distribution of rising SST. Given that most IPCC models project a larger increase in SST in the ENA than in the WNA, the projected eastward shift in TC genesis is likely to be robust.

1. Introduction

Tropical cyclones (TCs) were the most costly natural disaster to affect the United States over the period 1960–2005 (Peterson et al. 2008). In recent years, Hurricane Katrina (2005) was the most damaging storm (Schmidlin 2006), and Hurricane Wilma (2005) was the most intense storm (central pressure of 882 hPa) on record in the North Atlantic (NA). Hurricane Rita (2005) was the most intense (central pressure of 895 hPa) tropical cyclone ever observed in the Gulf of Mexico.

Hurricane activity in the NA showed an increase over the past 30 years (Goldenberg et al. 2001; Webster et al. 2005; Bell and Chelliah 2006). The increased severity of TCs has aroused public interest regarding the impact of global warming on TC activity. Previous studies have proposed that these recent changes are largely due to global warming (Emanuel 2005; Anthes et al. 2006; Hoyos et al. 2006; Mann and Emanuel 2006; Trenberth and Shea 2006; Holland and Webster 2007; Mann et al.

* School of Ocean and Earth Science and Technology Publication Number 7911.

+ Current affiliation: Japan Agency for Marine-Earth Science and Technology, Yokosuka, Japan.

Corresponding author address: Hiroyuki Murakami, Meteorological Research Institute (MRI), 1-1, Nagamine, Tsukuba-shi, Ibaraki 305-0052, Japan.
E-mail: himuraka@mri-jma.go.jp

DOI: 10.1175/2010JCLI3338.1

2007a, 2007b). However, this view has been challenged by the following points: 1) recent increases in the frequency of Atlantic TCs are within the range of observed multidecadal variability (e.g., Goldenberg et al. 2001; Pielke et al. 2005; Bell and Chelliah 2006) and 2) the observational data used to attribute the trend to global warming are insufficient (Landsea et al. 2006; Landsea 2007).

Many studies have sought to project the future climate associated with warmer sea surface temperature (SST) using increased-CO_2 scenarios and global circulation models (GCMs; Broccoli and Manabe 1990; Haarsma et al. 1993; Bengtsson et al. 1996; Krishnamurti et al. 1998; Royer et al. 1998; Sugi et al. 2002; Tsutsui 2002; McDonald et al. 2005; Chauvin et al. 2006; Oouchi et al. 2006; Yoshimura et al. 2006; Bengtsson et al. 2007; Gualdi et al. 2008; Zhao et al. 2009), and regional climate models (RCMs; Knutson et al. 1998, 2008; Knutson and Tuleya 1999, 2004; Nguyen and Walsh 2001; Walsh et al. 2004; Stowasser et al. 2007). Most of these studies predicted a future increase of TC intensity. Most models have also predicted a reduced frequency of TCs globally, with a wide range of predictions among models. Consequently, the Intergovernmental Panel on Climate Change (IPCC) Fourth Assessment Report (AR4; IPCC 2007) concluded in its summary chapter for policymakers that there is ''less confidence'' in projections of a global decrease in the frequency of TCs than in projections of increased maximum intensities. The inconsistency in future changes in TC frequency becomes more pronounced when specific tropical ocean basin is considered. For example, among 14 (12) previous numerical studies of future TCs over the NA [western North Pacific (WNP)], 5 (5) explicitly indicated an increasing frequency, whereas 9 (7) reported a decreasing frequency.

Although many modeling studies have explored future change in TC intensity or genesis frequency, few have considered present-day variation and future change in TC tracks. Based on an observational study, Wu et al. (2005) first noticed that in the WNP, TCs have experienced an eastward shift of the two prevailing northward recurving tracks over the period 1965–2003 due to interdecadal change in large-scale steering flows. Vecchi and Knutson (2008) showed a decrease in TC activity in the western part of the NA, and an increase in the eastern part over the past 100 years. It is important to investigate whether anthropogenic warming influences TC density over the NA.

Bengtsson et al. (2007) documented the TC track change from the end of the twentieth century to the end of the twenty-first century, based on an atmospheric general circulation model (AGCM) with T63 and T213 resolution. Although the global spatial patterns of future change of TC tracks were similar, the two resolutions predict different patterns in the eastern Pacific and NA. The authors attributed this inconsistency to inadequate TC genesis in the lower-resolution (T63) model, suggesting the importance of using very high-resolution models. Knutson et al. (2008) used a nonhydrostatic regional model with a grid spacing of 18 km forced by boundary conditions computed from the multimodel ensemble mean of Coupled Model Intercomparison Project (CMIP3; Meehl et al. 2007) under the A1B emission scenario, and found a decrease in TC occurrence in the western NA, due mainly to increased vertical shear and decreased midtropospheric relative humidity. The authors argued for the likelihood of a future change in TC genesis but did not discuss changes in the tracks associates with large-scale steering flows, which could also affect TC density. Chauvin et al. (2006) used a stretched-grid global model with 0.5° grid spacing over the NA and reported a future northeastward shift in TC activity; however, it remains unknown which factors are responsible for these changes in TC activity, although the authors reported that future change in TC frequency was identified by the Genesis Potential Index (GPI). In any event, the projected future changes in TC tracks remain uncertain because of the insufficient model resolution, the model biases in TC genesis and tracks, and the sensitivity of TC activity to the lateral boundary forcing and the spatial pattern of prescribed SST anomalies.

Since the current generation of models lacks the horizontal resolution necessary to resolve realistic TCs, an alternative approach is to infer tropical cyclone tracks from the output of the large scale wind field of global models. Wu and Wang (2004) proposed a synthetic ''trajectory model'' in which the future tracks of TCs at a given grid point are calculated from the mean beta drift and large-scale steering flows. However, they did not consider future changes in the genesis locations of TCs. A more sophisticated statistical–dynamical downscaling model was proposed by Emanuel (2006) and Emanuel et al. (2008). When applied to simulation of future change, this method predicts substantial changes and shifts in tropical cyclone activity, but with much variation among the global models used.

It is preferable to scrutinize model-simulated TCs in very high-resolution models when evaluating future change in TC climatology. The present study investigates future changes in TC activity, especially changes in TC tracks using a 20-km-mesh AGCM. The geographic focus is the NA. The model is similar to that used by Oouchi et al. (2006), but the experiment design is improved and the time integration increases from 10 to 25 yr. In Oouchi et al. (2006), the present-day experiment was forced by climatological observed SST and the future experiment was forced by SSTs predicted by a single model;

that is, the Meteorological Research Institute (MRI)-coupled atmosphere–ocean general circulation model (CGCM) 2.3 (Yukimoto et al. 2006). In contrast, the present study compares a pair of 25-yr experiments: the present-day experiment (1979–2003) was forced by observed SST including year-to-year variations and the future experiment (2075–2099) was forced by multimodel ensemble SST projected by 18 CMIP3 models (see details in section 2). Recent studies (e.g., Emanuel et al. 2008; Zhao et al. 2009) have suggested that the future changes in TC frequency in a specific basin show wide variation depending on the individual model's SST (or large-scale condition). Therefore, the use of the ensemble mean of SSTs may lead to a more reliable projection. The new design also includes year-to-year variation in SST forcing, as TC frequency and spatial distribution show large year-to-year variability in association with El Niño–Southern Oscillation (ENSO) in the NA (Gray 1984), and it is preferable that climate projections contain year-to-year variations in the prescribed SST.

Section 2 describes the model, simulation settings, and observational datasets. Section 3 outlines the analytical methods, including TC detection and the GPI, and section 4 provides details on model performance in the present-day simulation. Section 5 describes the simulation results in terms of future changes in TCs, and section 6 examines the reasons for the predicted future changes. The last section provides a summary of the main findings.

2. Model and experimental design

a. MRI/JMA 20-km-mesh AGCM

The climate model used in this study is the 20-km-mesh Meteorological Research Institute (MRI)/Japan Meteorological Agency (JMA) AGCM. A brief description of the model is given here; detailed accounts can be found in Mizuta et al. (2006) and JMA (2007). The MRI/JMA-AGCM is a hydrostatic and spectral AGCM with a resolution of T959L60 (triangular truncation 959 with a linear Gaussian grid, which is equal to 20-km mesh horizontally and 60 layers vertically). The model adopts a semi-Lagrangian scheme (Yoshimura and Matsumura 2003) that enables integration with a time step of 6 min. Regarding physics, the MRI/JMA-AGCM is equipped with a prognostic Arakawa and Schubert cumulus convection scheme (Randall and Pan 1993), a prognostic cloud scheme (Smith 1990), the level-2 turbulence closure scheme of Mellor and Yamada (1974) for vertical turbulent diffusion, a multiparameter random model for terrestrial radiation (Shibata and Aoki 1989), a delta-two-stream approximation scheme for solar radiation (Shibata and Uchiyama 1992), an orographic gravity wave drag scheme (Iwasaki et al. 1989), and a Simple Biosphere scheme (SiB) for a land surface model (Sellers et al. 1986; Sato et al. 1989).

The MRI/JMA-AGCM has been used for both medium-range forecasts at the JMA (JMA 2007; Murakami and Matsumura 2007; Murakami et al. 2008) and climate projections at the MRI (Kusunoki et al. 2006; Mizuta et al. 2006; Oouchi et al. 2006). Murakami et al. (2008) verified the performance of the model in simulating typhoons with real initial conditions and compared the results with those obtained by using a lower-resolution version of the model. The high-resolution version simulated more realistic tracks, intensity, and inner-core structure of typhoons. The increased accuracy is obtained mainly from increased horizontal resolution (Murakami et al. 2008). The performance of the model in climate simulations of TCs has been reported by Oouchi et al. (2006), who showed that the general features of TCs, including intensity and genesis frequency, are well simulated in a 10-yr present-climate simulation forced by prescribed climatological SST.

b. Simulation setting and boundary conditions

The multiyear climate simulations performed in this study were based on the so-called time slice experiments (Bengtsson et al. 1996), in which SST, sea ice concentration (SIC), and greenhouse gases are given as external forcings. To evaluate the future change in TC activity, two 25-yr simulations were performed for 1979–2003 period (the present day; PD) and the last quarter of the twenty-first century (2075–2099; global warming; GW). For the PD run, the Hadley Centre observational SST and SIC (HadISST1; Rayner et al. 2003) were prescribed, with the monthly mean data being interpolated to daily values. This approach differs from that adopted by Oouchi et al. (2006), who employed climatological annual cycle SST and SIC. The observed SSTs contain interannual variation, such as ENSO, which is the most influential factor in terms of TC variations (Camargo et al. 2007a).

For the GW run, the future SST and SIC were created following the method described by Mizuta et al. (2008; Fig. 1). First, observed SST and SIC were decomposed into a trend (PDTR) component and an interannual variation (PDIV) for the 25 years from 1979 to 2003. Second, the same decomposition was applied to the ensemble mean of the World Climate Research Program/CMIP3 models (here, 18 models were used as listed in Table 1), thereby obtaining the future trend (GWTR) and interannual variation for the 25 years from 2075 to 2099. The average values of SST and SIC for each period were also calculated so that the future change (GWDT) was computed. Finally, the future forcing conditions were reconstructed as a recomposition of GWDT, GWTR, and PDIV. Note that here the amplitude and phase of

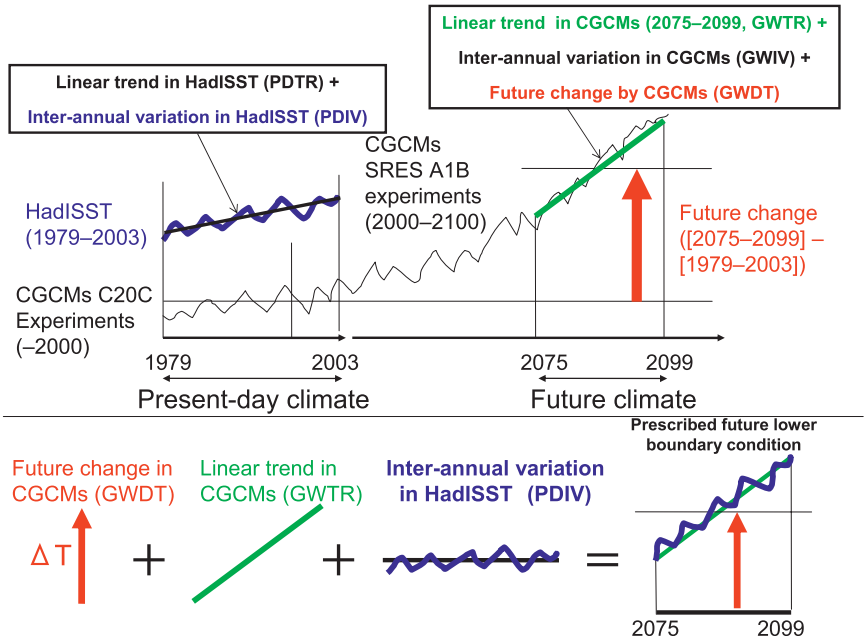

FIG. 1. Schematic diagram of prescribed lower boundary conditions for the future simulation. The abbreviations are expanded in text except for GWIV: interannual variation in the ensemble mean of future SSTs and C20C: climate of the twentieth century.

the interannual variation are assumed to be conserved in the future setting. We did not use the raw time series of the multimodel ensemble mean because the averaging smoothes out year-to-year variability of SST and excludes ENSO.

The annual concentrations of greenhouse gases (CO_2, CH_4, and N_2O) were derived from observed values for the PD run, and from the A1B IPCC emission scenario (IPCC 2007) for the GW run. For aerosols, the climatological monthly mean values were calculated from the global chemical transport model (Tanaka et al. 2003). The same aerosols were also used for the GW run.

c. *Observational best-track data*

The global TC dataset, obtained from the Web site of Unisys Corporation (Unisys 2009), was used to evaluate TC simulations in the PD run. The dataset consists of best-track data compiled by the National Hurricane Center (NHC) and Joint Typhoon Warning Center (JTWC), and contains historical TC information regarding the center location, intensity (maximum 1-min surface wind speed), and sea level pressure in the NA at 6-h intervals from 1851 to 2009. We used only the TCs with tropical storm intensity or stronger (i.e., TCs that possess 1-min sustained surface wind of 35 kt or greater).

d. *JRA-25 reanalysis data*

The Japanese 25-yr Re-Analysis (JRA-25) dataset (Onogi et al. 2007) was used for the GPI analysis. The JRA-25 reanalysis system was constructed based on the former global operational forecast and assimilation system at the JMA. The system consists of a three-dimensional variational data assimilation (3DVAR) and a spectral forecast model with a resolution of T106L40 (triangular truncation at wavenumber 106 in the horizontal and 40 vertical layers). The data available period is from 1979 to 2004. One of the advantages of the JRA-25 is that it adopted TC retrieved (TCR) data in the assimilation process (Hatsushika et al. 2006). The TCR data provide an artificial three-dimensional TC structure constructed using information from the best-track data, such as position, motion, maximum surface winds, and the radii of 30- and 50-kt wind speeds. The TCR was then treated as observational data in the assimilation process. This approach yields both realistic environmental flows around a TC and TC structure. Several variables were used in the GPI calculation (see section 3b); however, because the vertical motion (omega) is not included in the reanalysis field, we used the omega in the first-guess field (i.e., the model output in the assimilation process).

3. Analysis methods for projected outputs

a. *Detection method for tropical cyclones*

The TC-detection method adopted in the present study is a modified version of that used by Oouchi et al. (2006), who employed six criteria to identify TCs in order to match the simulated annual mean number of global TC

TABLE 1. CMIP3 Models used for future prescribed boundary conditions.

Name	Institute
BCCR_BCM2_0	Bjerknes Centre for Climate Research, Norway
CGCM3.1 T47	Canadian Centre for Climate Modeling and Analysis, Canada
CGCM3.1 T63	
CNRM CM3	Météo-France/Centre National de Recherches Météorologiques, France
CSIRO Mk3.0	CSIRO Atmospheric Research, Australia
GFDL CM2.0	Geophysical Fluid Dynamics Laboratory/NOAA/U.S. Dept. of Commerce, United States
GFDL CM2.1	
GISS AOM	Goddard Institute for Space Studies, National Aeronautics and Space Administration, United States
INM CM3.0	Institute for Numerical Mathematics, Russia
IPSL CM4	Institut Pierre Simon Laplace, France
MIROC3.2 hires	Center for Climate System Research (University of Tokyo), National Institute
MIROC3.2 medres	for Environmental Studies, and Frontier Research Center for Global Change (JAMSTEC), Japan
MIUB ECHO-G	Meteorological Institute of the University of Bonn, Meteorological Research Institute of KMA, and Model and Data Group, Germany and Korea
MPI ECHAM5	Max Planck Institute for Meteorology, Germany
MRI CGCM2.3	Meteorological Research Institute, Japan
NCAR CCSM3.0	National Center for Atmospheric Research, United States
UKMO HadCM3	Hadley Centre for Climate Prediction and Research/Met Office, United Kingdom
UKMO HadGem1	

genesis with observations. However, the simulated TC numbers in each ocean basin do not agree with observations. The present-day simulation performed by Oouchi et al. (2006) shows that the TC number was markedly underestimated in the WNP, somewhat underestimated in the NA, and significantly overestimated in the South Indian Ocean. In the present study, given that we focus on changes in TC tracks over the NA, the detection criteria were modified to ensure that the simulated annual number and duration of TCs resemble the observed counterparts. The modified detection criteria are as follows:

1) Across the latitudinal belt of 45°S–45°N, the grid point of the candidate TC center is defined as that where the minimum surface pressure is at least 2 hPa lower than the averaged surface pressure over the surrounding 7° × 7° grid box.
2) The magnitude of the maximum relative vorticity at 850 hPa exceeds 3.0×10^{-5} s^{-1} (original value: 3.5×10^{-5} s^{-1}).
3) The maximum wind speed at 850 hPa exceeds 14.0 m s^{-1} (original value: 15.0 m s^{-1}).
4) The temperature structures aloft show a marked warm core: the sum of the temperature deviations at 300, 500, and 700 hPa exceeds 1.2 K (original value: 2 K).
5) The maximum wind speed at 850 hPa (WS850) exceeds that at 300 hPa (WS300) at the first detection (i.e., generation time) of a TC. After generation, WS850 increased by 2.5 m s^{-1} should be greater than WS300 (this latter condition was not required in the original detection).
6) The duration of a TC exceeds 36 h.

Conditions 1 and 6 are the same as the original conditions employed by Oouchi et al. (2006), whereas conditions 2–5 have been modified. The latter part of condition 5 results in a greater number of TC occurrence at midlatitudes. This criterion is added because a comparison of simulated TC tracks with observed track data reveals that the model underestimates the number of TC tracks at midlatitudes in the case that this relaxation is not employed. It might be argued that this relaxation would increase the number of extratropical cyclones; however, this condition is only valid for TCs generated at low latitudes. In other words, we only select those cyclones with transient characteristics that were generated at low latitudes. We included these transitional TCs because evaluation of their future changes is important when estimating the future socioeconomic costs arising from TC-related damage.

The model TC positions were counted for every 2.0° × 2.0° grid point over the NA region (0°–45°N, 110°W–0°, excluding the Pacific) every 6 h. The total count was defined as the frequency of TC occurrence, which indicates the probability of a TC occurring in a certain grid point. When the counting is only applied to genesis location (i.e., when initially identified according to the detection method), the total number of TCs is defined as the frequency of TC genesis. Because TCs in the NA are generated mainly during the boreal summer (July–October; JASO), this study primarily focuses on changes in TC tracks during these months.

b. *Emanuel and Nolan's Genesis Potential Index*

To determine the factors responsible for genesis location changes, we used the Genesis Potential Index

originally developed by Emanuel and Nolan (2004), motivated by the work of Gray (1979). Although the GPI was developed using a statistical fitting procedure, based only on climatological seasonal and spatial variations in TC genesis, it shows some skill in reproducing interannual variations in the observed frequency and location of TC genesis for several basins (Camargo et al. 2007a). GPI values increase when large-scale conditions are favorable for TC genesis and decrease when conditions are unfavorable. The formulation of the original GPI is as follows:

$$\mathrm{GPI} = \left|10^5\eta\right|^{3/2}\left(\frac{\mathrm{RH}}{50}\right)^3\left(\frac{V_{\mathrm{pot}}}{70}\right)^3(1+0.1V_s)^{-2}, \quad (1)$$

where η is the absolute vorticity (s^{-1}) at 850 hPa, RH is the relative humidity (%) at 700 hPa, V_{pot} is the maximum potential intensity (m s^{-1}) of Emanuel (1995), and V_s is the magnitude of the vertical wind shear (m s^{-1}) between 850 and 200 hPa. Among these factors, only vertical wind shear is negatively correlated with the GPI. The relative humidity and maximum potential intensity are considered thermodynamical factors. The maximum potential intensity is an empirical value, and is determined by the vertical structure of temperature and moisture, and SST. The definition of maximum potential intensity is based on Emanuel (1995), as modified by Bister and Emanuel (1998). Camargo et al. (2007a) calculated the GPI using reanalysis data, showing good agreement between observational data and the climatology and ENSO-related variability in GPI. Camargo et al. (2007b) applied the GPI to model outputs. The GPI is used not only to provide supplemental information regarding TC genesis estimated from model simulations, but also to clarify the most influential factor in the case of GPI variation due to ENSO or the case of differences identified when comparing different models.

When the original GPI was applied to JRA-25 data, we found significant discrepancies between the GPI (Fig. 2a) and the observed distribution of TC genesis (Fig. 2c). First, the original GPI underestimates the frequency of genesis in the intertropical convergence zone (ITCZ) between 7° and 15°N. Second, the GPI underestimates the frequency of TC genesis in the eastern Pacific.

It is expected that TC generation is strongly related to large-scale mean vertical motion. Indeed, our analysis reveals that regions with a high frequency of TC genesis correspond to areas with large upward motion. It is possible that upward motion was not fully taken into account in the original GPI, although the relative humidity term may reflect it to some degree. In the present study, we modified the original GPI by explicitly incorporating the following vertical motion term:

$$\mathrm{GPI}' = \left|10^5\eta\right|^{3/2}\left(\frac{\mathrm{RH}}{50}\right)^3\left(\frac{V_{\mathrm{pot}}}{70}\right)^3(1+0.1V_s)^{-2}\left(\frac{-\omega+0.1}{0.1}\right), \quad (2)$$

where ω is the vertical wind velocity (Pa s^{-1}). Figure 2b shows the modified GPI, which yielded improved results in general, including higher values over the eastern Pacific and the Atlantic ITCZ region. However, the modified GPI remains inconsistent with observations of TC genesis around the Florida peninsula and off the coast of West Africa. This inconsistency also appears when the modified GPI is applied to model output (as shown later in Fig. 9). Although further improvement of the GPI may be needed, we found that the modified GPI shows future change in detected TC genesis more clearly than did the original GPI.

No other study has applied GPI analysis to such a high-resolution simulation. A concern might naturally arise that the vertical motion field induced by TCs may contribute to the seasonal mean field. Although the degree to which TCs affect climatological mean vertical motion remains unclear, it is conceivable that the influence is rather limited, given that fact that on average only nine storms occur during the four-month peak season. On the other hand, the incorporation of vertical motion into the GPI provides additional information regarding the physical mechanism for future change in TC genesis.

4. Evaluation of the present-day simulation

a. TC tracks and frequency of occurrence

To evaluate the TC climatology and variations simulated in the PD run, we compared the results with observations. Figures 3a,b (Figs. 3c,d) show JASO TC tracks (frequency of occurrence) observed and simulated in the PD run, respectively. The difference between the observed and simulated (PD run) frequency of occurrence is shown in Fig. 3e. Overall, the simulated TC tracks and frequency of occurrence are similar to the corresponding observations; however, the PD run overestimates the frequency of occurrence in tropical regions (south of 25°N), and underestimates the frequency north of 25°N. The underestimation mainly reflects a lack of cyclogenesis within midlatitude regions in the PD run. The PD run also underestimates TC genesis over the Gulf of Mexico and the frequency of TCs moving northward from this region, and overestimates the frequency of occurrence in the region offshore from West Africa.

b. Interannual and seasonal variability in TC genesis

Because the prescribed SST and SIC vary from year to year, we expect to see a corresponding interannual

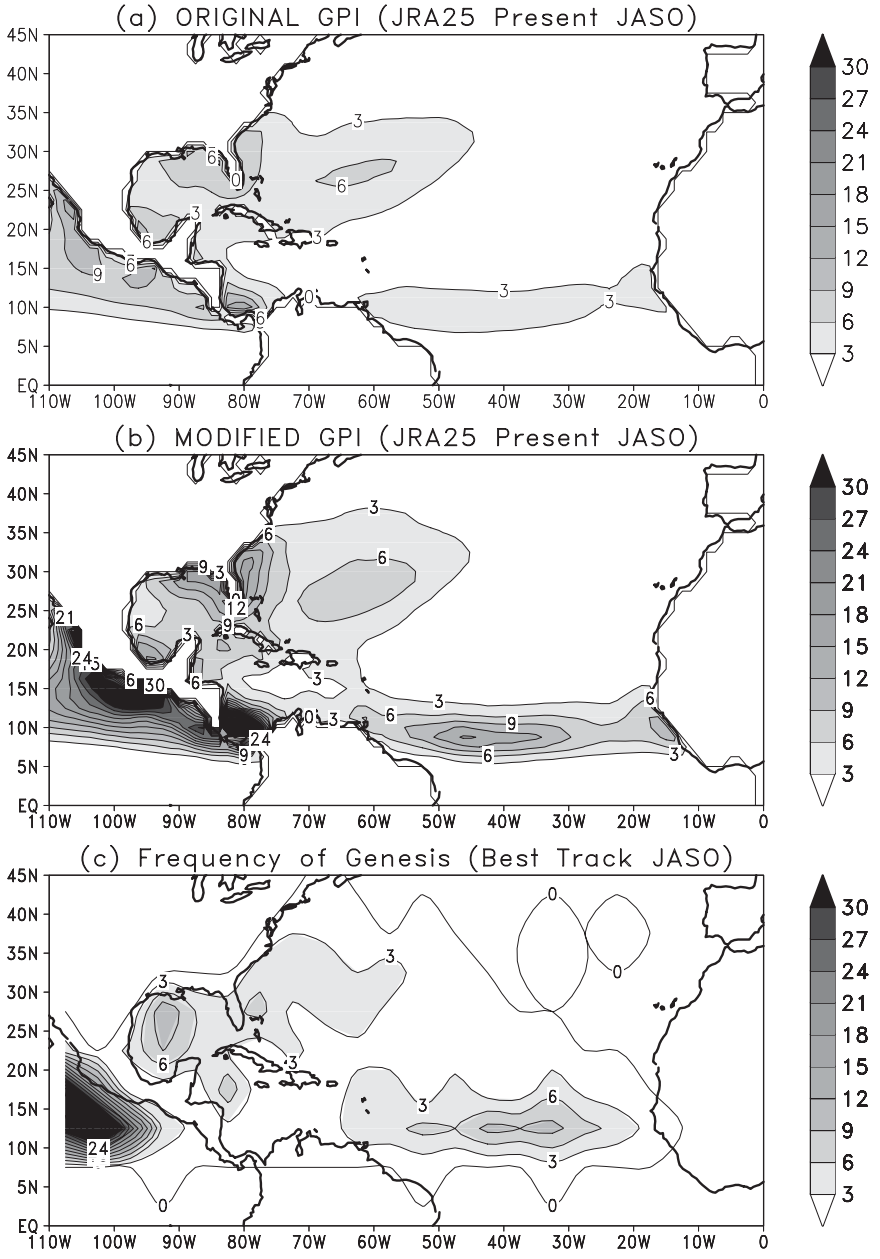

FIG. 2. JASO mean of (a) original GPI, (b) modified GPI, and (c) frequency of TC genesis based on best-track data in the NA. The GPI data were calculated using JRA-25 reanalysis data for the period 1979–2003.

variation in TC genesis in the PD run. Figure 4a compares the simulated and observed yearly number of TC genesis. The average numbers of TC genesis are 10.5 (observed) and 8.7 (PD run), meaning that the total number of TCs is underestimated. The recently observed upward trend in TC genesis, which is conspicuous from the mid-1990s, is insufficiently reproduced in the PD run. The coefficient of correlation between the PD run and observations is 0.46, which is statistically significant at the 95% level. Therefore, to some degree, the PD run reproduces the observed year-to-year variation in TC genesis number. However, this correlation is weaker than that reported in other studies. For example, LaRow et al.'s (2008) ensemble simulations using a global spectral model at a resolution of T126L27 (Gaussian-grid spacing of 0.94°) yielded a correlation coefficient of 0.78. Zhao et al.'s (2009) ensemble simulations using a global atmospheric model with a 50-km horizontal-grid spacing yielded

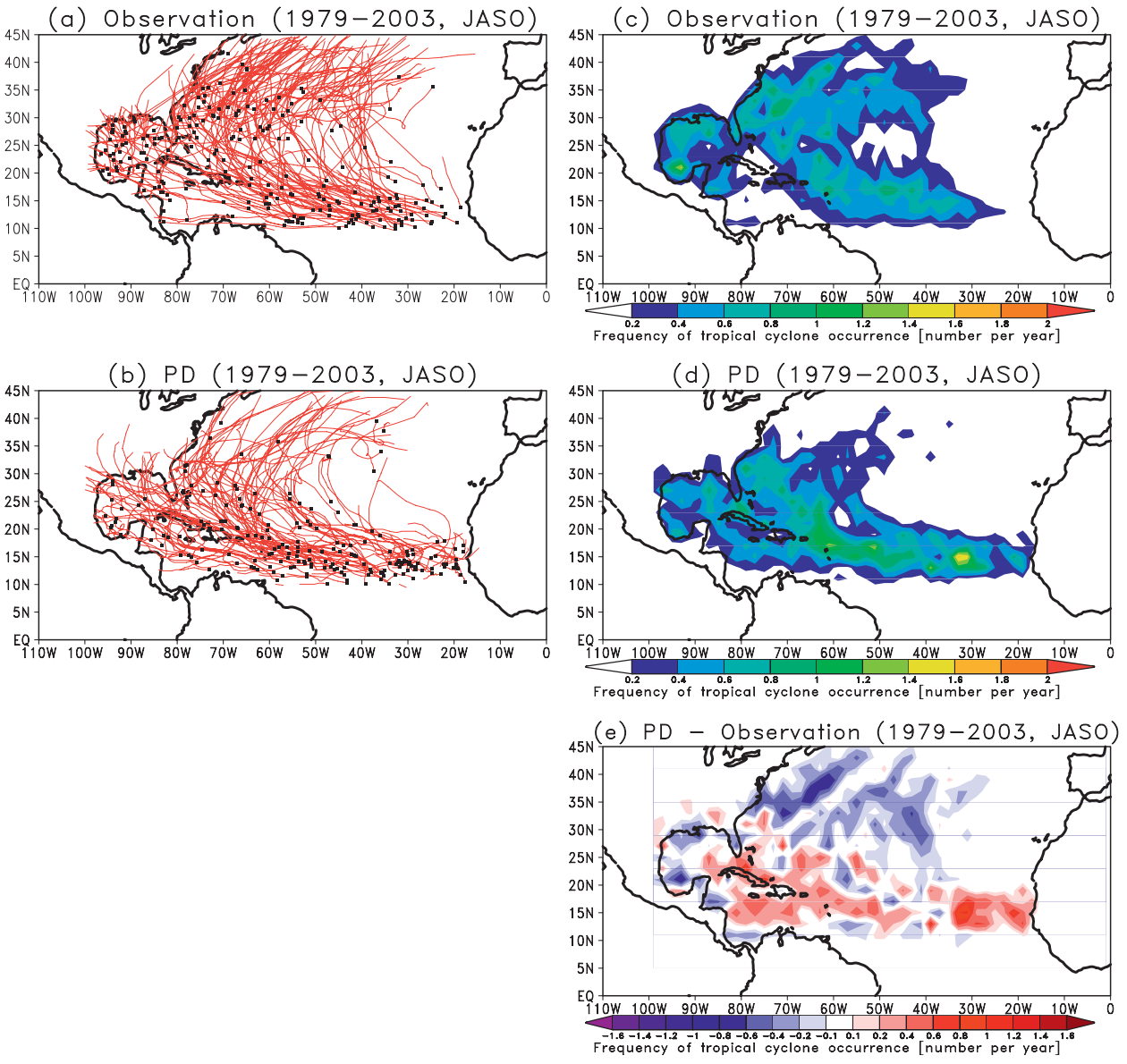

FIG. 3. (a),(b) Total tropical cyclone tracks and (c)–(e) frequency of occurrence for JASO from 1979 to 2003 in the NA; (a) and (c) are observed data, while (b) and (d) are data from the PD run. (e) The difference in frequency of occurrence between the PD run and observations. (a),(b) Black dots show TC-genesis locations.

a correlation coefficient of 0.83. We noticed that our result is derived from a single run; if the correlation is computed only for the last 15 (10) yr of the experiment, the correlation coefficient would increase to 0.65 (0.73).

Figure 4b shows seasonal variations in TC genesis. As in nature, the simulated TC genesis shows a rapid increase from June to July, peak in September, and a decrease toward the northern winter. This pattern of variation is well simulated in the PD run. Although LaRow et al. (2008) accurately reproduced the interannual variation in TC number, their seasonal cycle of TC number was not well simulated in the NA. In contrast, the experiment by Zhao et al. (2009) performed very well in reproducing both interannual variations and the seasonal cycle of TC number. These results, in combination with the present findings, suggest that model performance in simulating of interannual variations may be weakly related to performance in simulating the seasonal cycle.

c. *Change in TC activity induced by ENSO*

It is clear from Fig. 4a that the simulated TC number (PD run) is strongly affected by ENSO. For example, TC genesis shows a marked decline during El Niño years (1982, 1986, 1987, 1997, and 2002), consistent with the

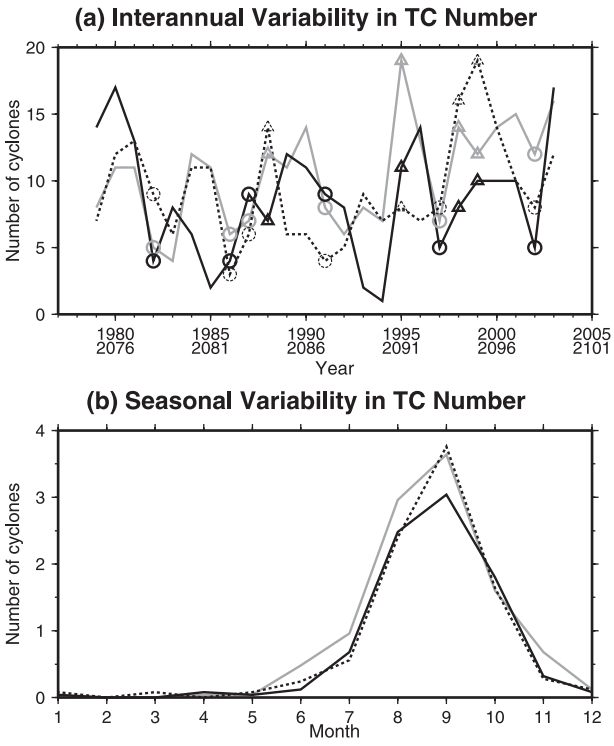

FIG. 4. (a) Yearly and (b) seasonal variability in the number of generated TCs, based on observations (1979–2003; solid gray line), the PD run (1979–2003; solid black line), and the GW run (2075–2099; dotted black line). The coefficient of correlation for yearly TC number between the PD run and observation is 0.46, which is statistically significant at the 95% level. The average annual numbers of TCs are 10.5 (observed), 8.7 (PD run), and 9.2 (GW run). (a) Circles (triangles) indicate El Niño (La Niña) years.

finding of Gray (1984), who attributed this decrease to enhanced vertical shear of zonal wind over the Gulf of Mexico and Caribbean Sea. In La Niña years (e.g., 1988, 1995, 1998, and 1999), TC genesis increases because of decreased vertical wind shear; however, this increase is poorly captured by the PD run. This deficiency in TC genesis is generally caused by a number of errors, such as those in the simulated large-scale environment field, and deficiencies in the model's teleconnection linking ENSO and Atlantic atmospheric anomalies. In addition, our integration is a single run. Use of ensemble simulation may get better results.

To clarify whether the AGCM employed in the present study contains large-scale errors, the modified GPI was applied to the PD run; it was also applied to the JRA-25 large-scale field to evaluate the influence of the ENSO signal on TC genesis. Figure 5 shows GPI anomalies and the locations of TC genesis in July–October for each ENSO-developing year. Here, El Niño (La Niña) years are defined as 1982, 1986, 1987, 1991, 1997, and 2002 (1988, 1995, 1998, and 1999), following Camargo and Sobel (2005). For JRA-25 and best-track data (Figs. 5a,b), marked differences are seen in both GPI and genesis locations. There exists a negative (positive) anomaly in GPI values and frequency of genesis during El Niño (La Niña) years in the main developing regions (MDR; 10°–20°N, 30°–80°W). This contrast in the GPI field between El Niño and La Niña years at lower latitudes (south of 20°N) is reflected in the PD run (Figs. 5c,d), although the GPI signal is different from observations in areas offshore from West Africa in La Niña years. This finding indicates that MRI/JMA AGCM, at least to some extent, simulates differences in the large-scale field between El Niño and La Niña years, which affects TC genesis. The locations of TC genesis in the PD run also differ between the two ENSO phases, although the difference is weaker than that observed. There also exists an inconsistency between the GPI and detected TCs in the PD run. For example, many TCs are generated in the region offshore from West Africa during El Niño years, whereas the corresponding GPI values are small. This overestimation is unrelated to large-scale field errors, although the exact reasons remain to be investigated.

5. Projected future change in TC tracks, frequency, and interannual variation

Figures 6a,b (Figs. 6c,d) shows JASO TC tracks (frequency of occurrence) simulated in the PD and GW runs, respectively. The difference in frequency of occurrence between the two runs is shown in Fig. 6e. Compared with the PD run, substantial changes are apparent in the GW run, including an increase in the frequency of TC occurrence over the tropical eastern North Atlantic and the northwestern North Atlantic (around 32°–45°N, 55°–80°W), and a decrease in the frequency over the tropical WNA (including the Caribbean Sea and Gulf of Mexico). This result indicates a decrease in the frequency of TCs that affect the North American continent south of approximately 32°N and the West Indies. To ensure the physical significance and robustness of the shifts in TC tracks, we implemented two additional analyses with different TC criteria: one used relatively constrained criteria (compared with the one used in the present study), as employed by Oouchi et al. (2006), and the other used less-constrained criteria. These two new sets of detection criteria result in very similar future change in TC tracks (data not shown), thereby demonstrating that the projected future change is independent of the TC criteria employed.

The dotted line in Figs. 4a,b shows interannual and seasonal variability for the future run, respectively. The annual mean number of TC genesis is 9.2, slightly higher

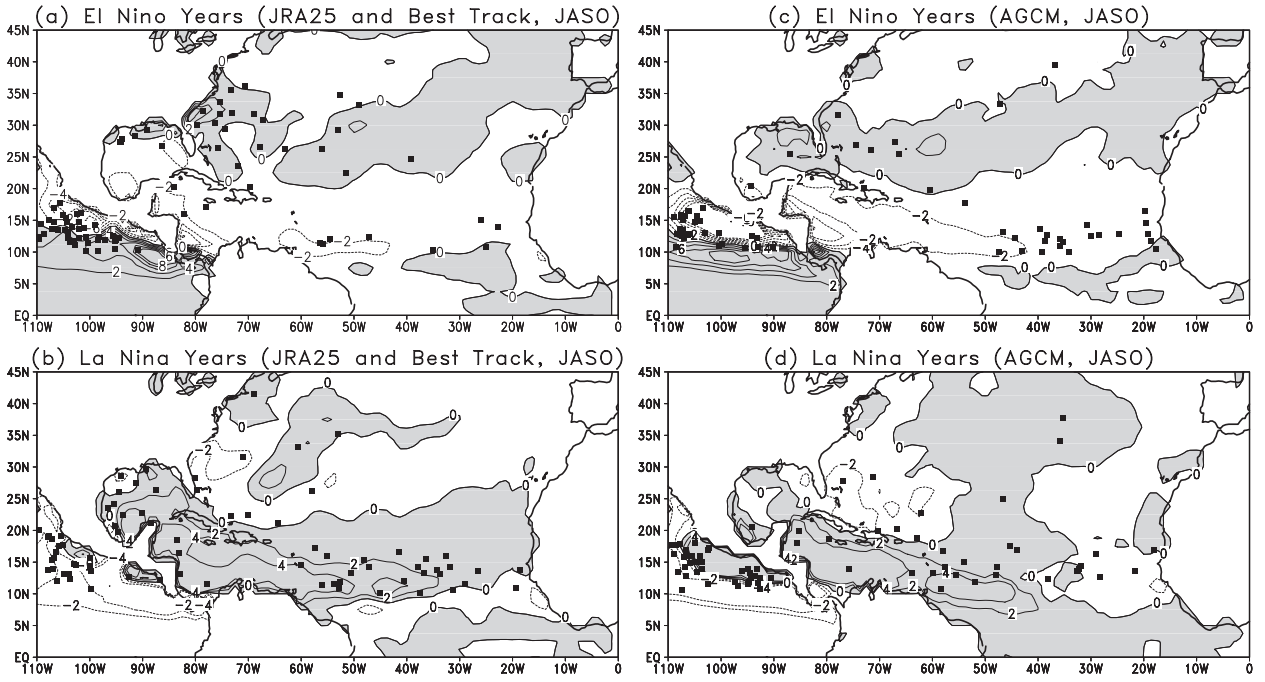

FIG. 5. Locations of TC genesis (squares) and GPI anomalies (contours) for JASO during (a),(c) El Niño years and (b),(d) La Niña years. Gray shading indicates a positive anomaly in GPI. (a),(b) GPI calculated from JRA-25 reanalysis and best-track data, and (c),(d) from the PD run. El Niño (La Niña) years are defined as 1982, 1986, 1987, 1991, 1997, and 2002 (1988, 1995, 1998, and 1999).

than that in the PD run, although the difference is not statistically significant at the 95% level. Oouchi et al. (2006) also showed increasing TC number over the NA in their future experiment. A resent study by Sugi et al. (2009), using the same MRI/JMA AGCM but with different resolutions, showed that future change in TC number within a specific ocean basin is strongly controlled by the distribution of relative SST changes rather than the absolute value of local SST. A similar finding was reported by Vecchi and Soden (2007a). Sugi et al. (2009) also reported an experiment that showed decreasing TC number over the NA with a relatively small future SST change in the NA. However, Knutson et al. (2008) and Zhao et al. (2009) reported decreasing TC number in their future experiment, when SST is prescribed by the same CMIP3 ensemble mean. Overall, the nature of future change in TC number in the NA remains uncertain, as also concluded by Emanuel et al. (2008).

Although the two runs prescribe similar interannual variations in SST and SIC, the interannual variation in the GW run (Fig. 4a) differs from that in the PD run. This discrepancy is more apparent in the first 20 years for the simulations. The interannual variation in TC number in the GW run is strongly affected by the specified ENSO (dotted line in Fig. 4a). For example, local minima occur in El Niño years (e.g., 2082, 2083, 2087, 2093, and 2098). Interestingly, the local maxima in La Niña years are more clearly resolved than those in the PD run (e.g., 2084, 2094, and 2095). The seasonal variation in TC frequency (Fig. 4b) is similar to that in the PD run, indicating no future change in seasonal distribution.

6. Reasons for future change

a. Reason for future change in TC tracks

The projected change in frequency of TC occurrence is thought to result from changes in steering flows or genesis locations. To help assess which of these two factors is more influential, JASO mean steering flows are shown in Fig. 7. Here, steering flows are defined as the pressure-weighted mean flow from 850 to 300 hPa, as suggested by Holland (1993). Overall, TC tracks (Figs. 6a,b) follow a combination of the steering flows and beta drift. The beta drift arises from interaction between the gradient of earth's vorticity and the primary TC circulation, which is generally westward and poleward. Tracks are followed by westward steering flows around the region offshore from West Africa, northwestward steering flows over the Caribbean Sea and Gulf of Mexico, and northeastward flows along the area offshore from North America. However, the PD and GW runs show only a small difference in steering flows (Fig. 7c), indicating that this is not a primary reason for the predicted change in frequency of TC occurrence. Furthermore, Fig. 8 shows

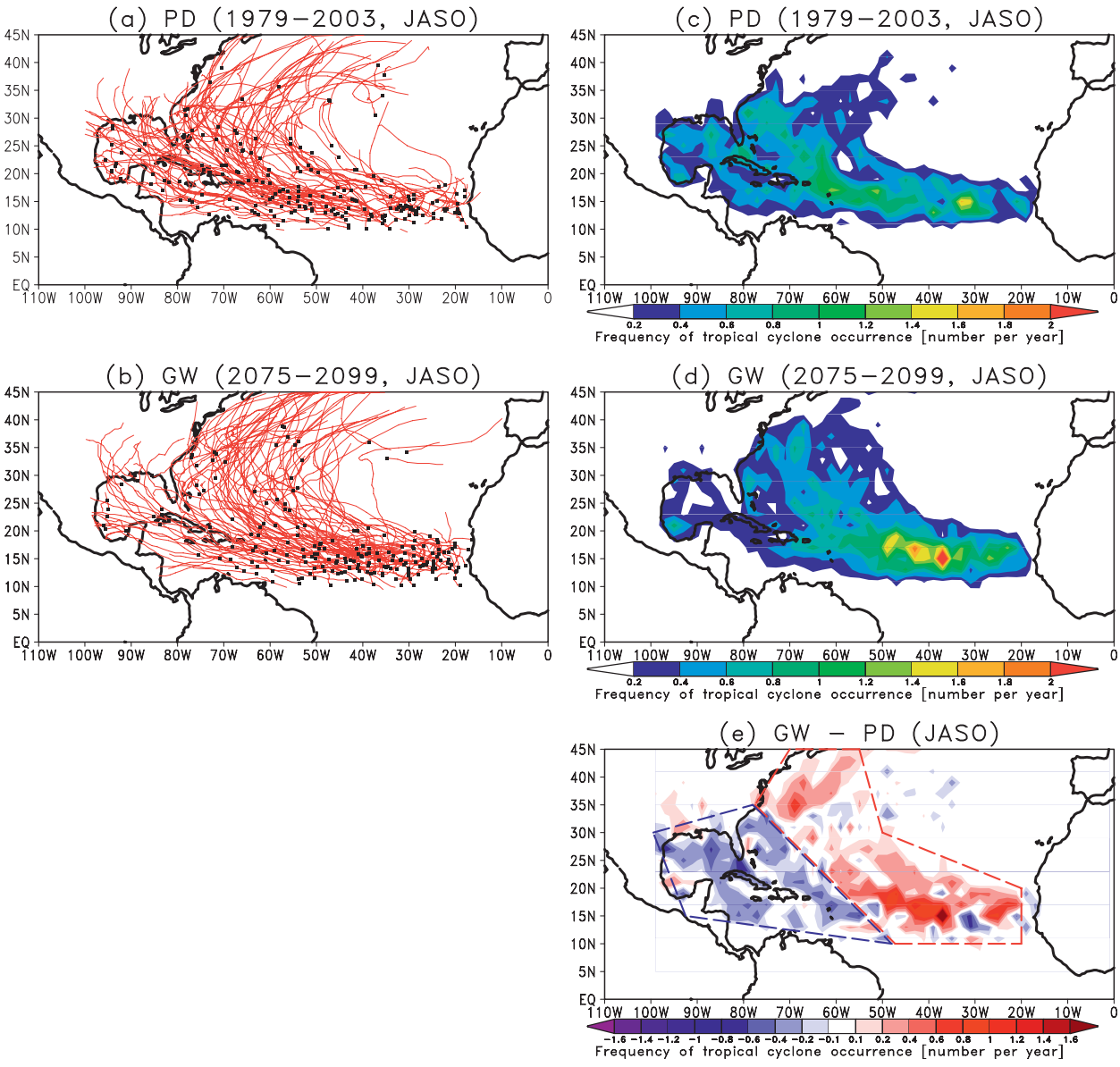

FIG. 6. As in Fig. 3, but between the PD and GW runs. (e) The dashed regions highlight an east–west contrast in future change of TC occurrence pattern.

a comparison of climatological mean TC translation vectors. The mean TC translation vectors are calculated at every 2.5° × 2.5° grid point based on all the TCs that passed across each point. The TC translation vectors are similar between the PD and GW runs, indicating that each TC moves in a similar direction for both runs for a given genesis location.

In contrast, there exist marked differences in genesis locations between the PD and GW runs. Figures 9a,b show the frequency of TC genesis during the peak cyclone season (JASO) for the PD and GW runs, respectively. The future change is shown in Fig. 9c. It is clear that the genesis locations shift eastward from the PD to GW runs, resulting in a large increase in TC genesis in the ENA and a decrease in the WNA. There is also an increasing signal in the NWNA. The increase in the frequency of TC genesis in the ENA indicates that many TCs experience early recurvature and then move northward, whereas the decrease in the WNA indicates a smaller risk of TCs approaching the coast of southeast United States. These changes appear to be consistent with the predicted change in frequency of TC occurrence (Fig. 6e), thereby indicating that the change of TC frequency is caused mainly by the change in genesis locations.

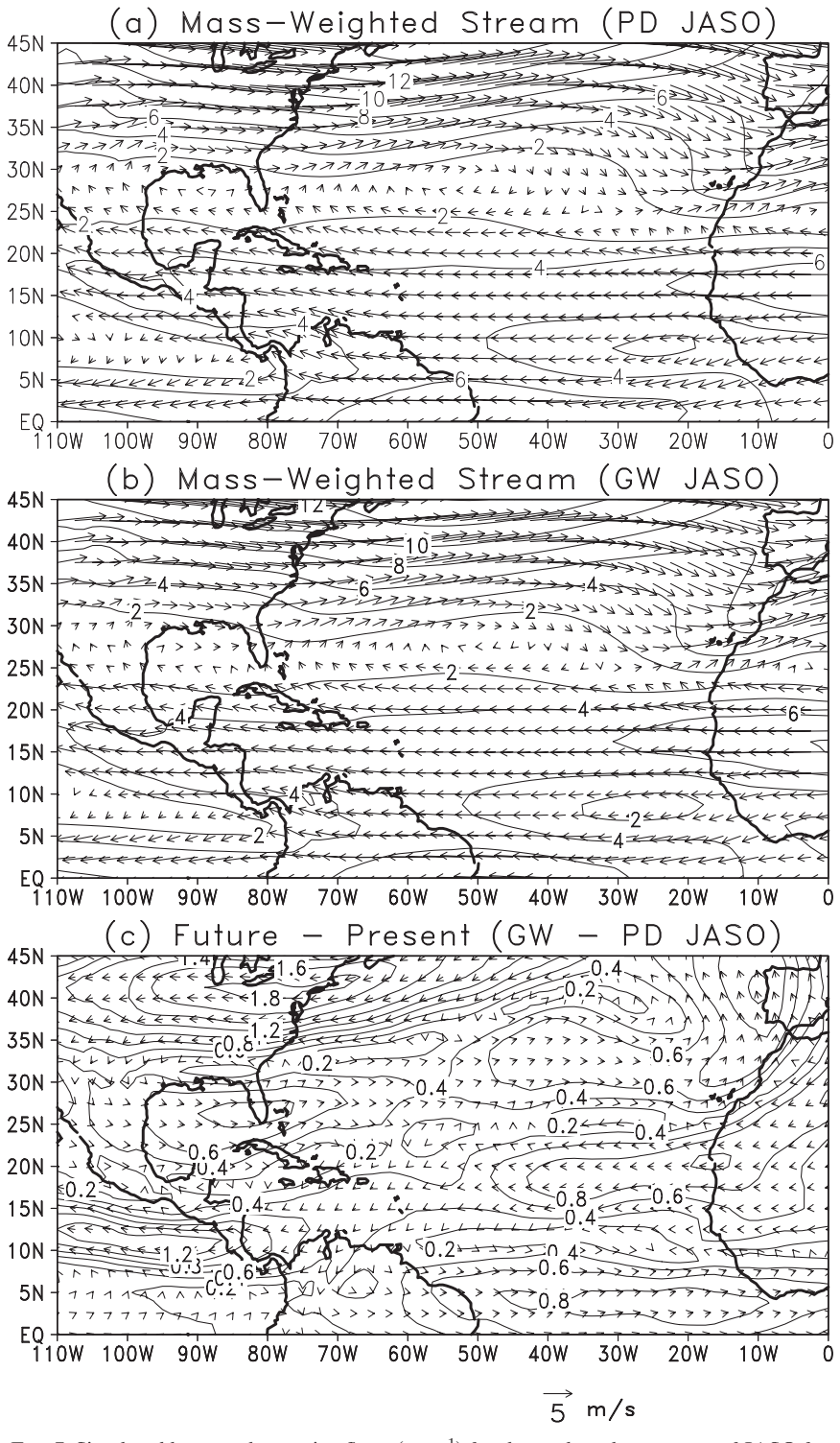

FIG. 7. Simulated large-scale steering flows (m s^{-1}) for the peak cyclone season of JASO for (a) the PD run, (b) the GW run, and (c) the difference between the GW and PD runs.

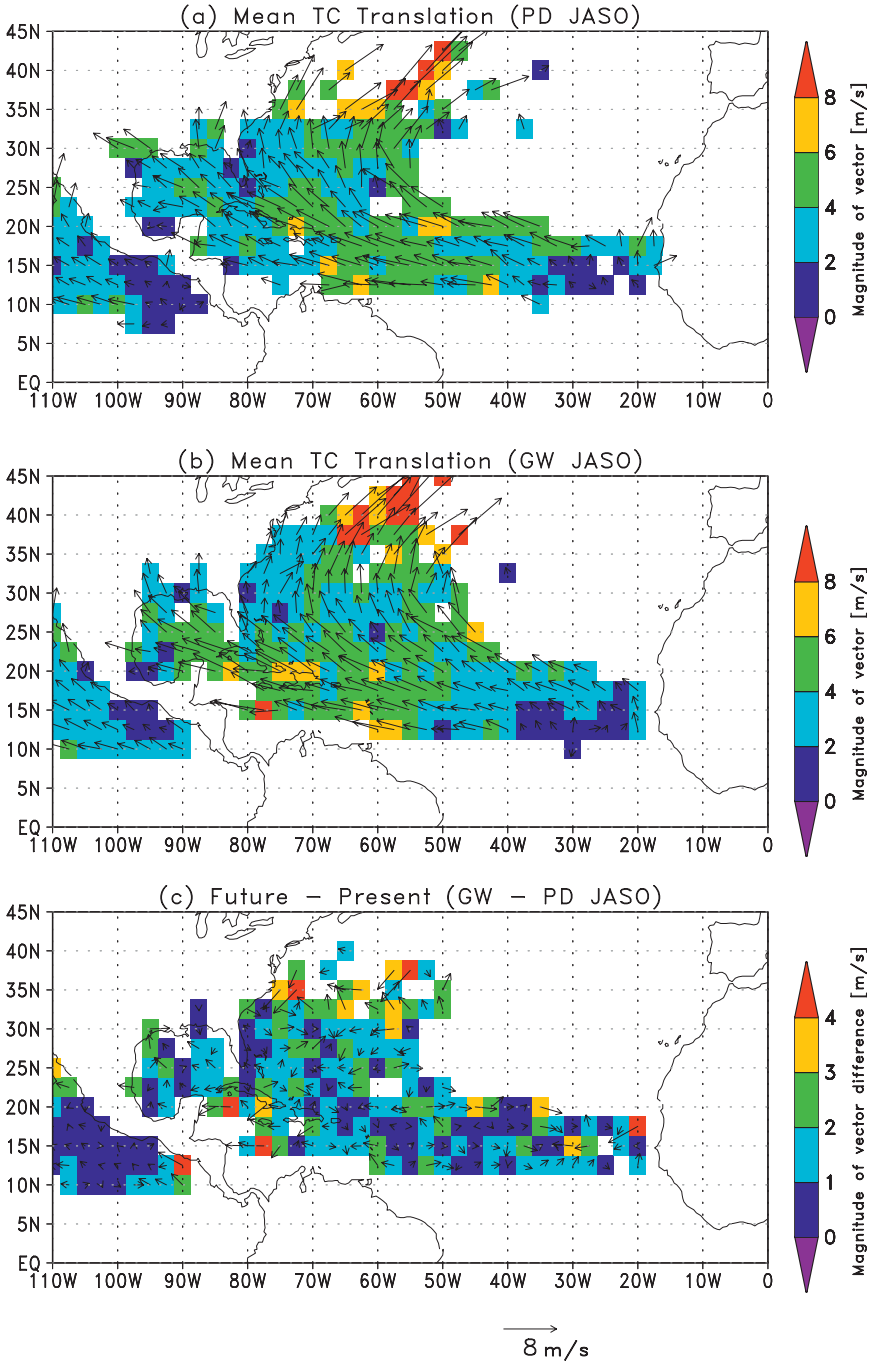

FIG. 8. Simulated mean TC translation vectors and magnitudes (m s^{-1}) for the peak cyclone season of JASO for (a) the PD run, (b) the GW run, and (c) the difference between the GW and PD runs. More than seven storms per each grid are required for the plots.

b. Reasons for future change in genesis locations

We investigate the reason for changes in genesis locations based on an analysis using the modified GPI. Figures 9d,e shows the GPI in JASO for PD and GW runs. When these data are compared with the frequency of genesis (Figs. 9a,b), the GPI performs reasonably well in capturing the distributions of detected genesis, although it shows large values in the area around the Florida peninsula, where TC genesis does not occur. When we compare future changes in the GPI (Fig. 9f) and frequency of genesis (Fig. 9c), the GPI change largely

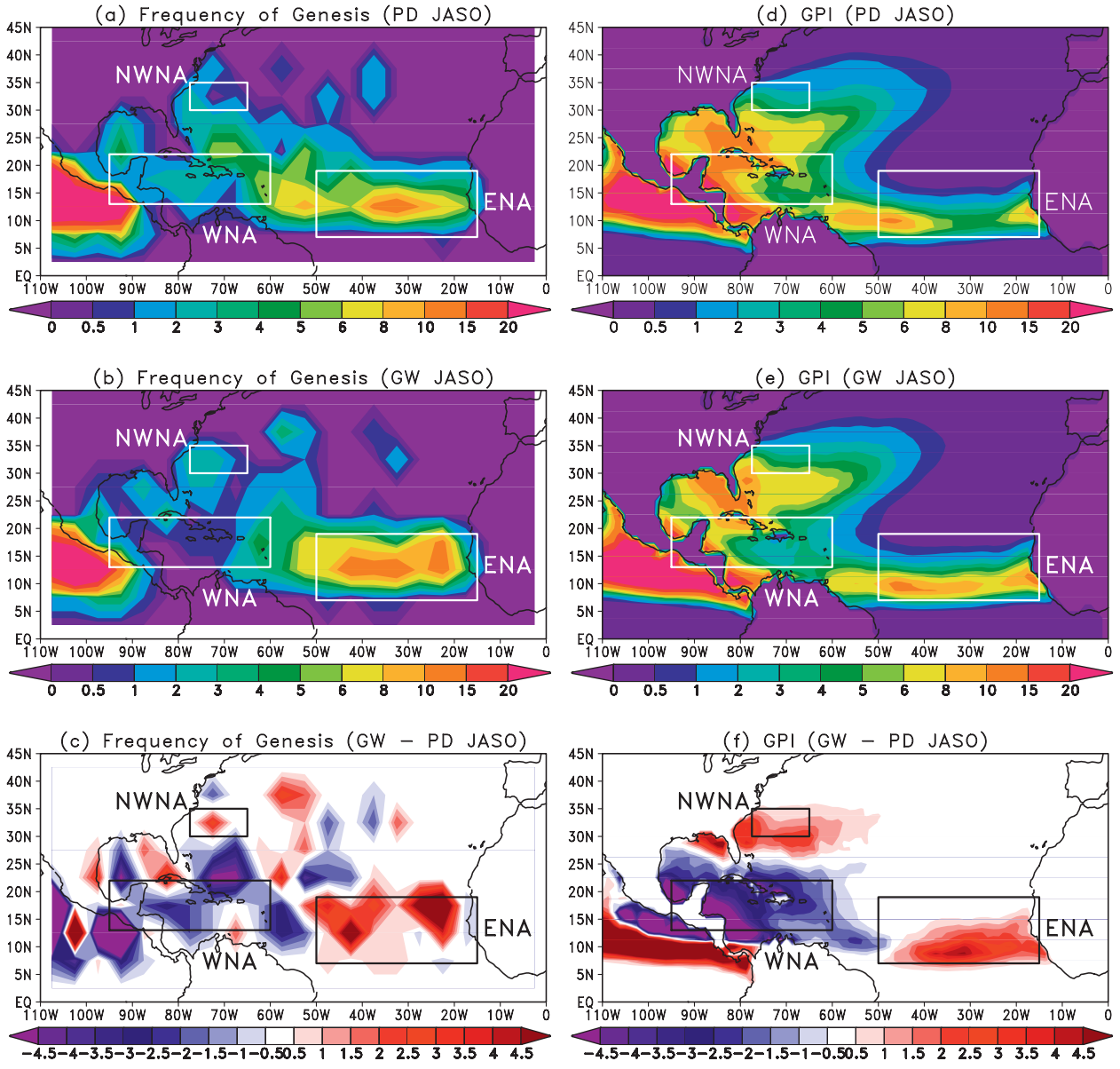

FIG. 9. Simulated frequency of TC genesis for the peak cyclone season of JASO for (a) the PD run, (b) the GW run, and (c) the difference between the GW and PD runs. (d)–(f) As in (a)–(c), but for the GPI. Rectangles show ENA, WNA, and NWNA with pronounced changes in TC genesis (see text).

captures the change in frequency of genesis. For example, contrasting changes in the frequency of genesis are found across the longitude 50°W, with an increase in the ENA and a decrease in the WNA. The GPI change also shows an increasing change in the NWNA.

The GPI can be used to determine which of the factors contributes most to its future change. Here, we assign the future value to one of the five GPI elements in Eq. (2); the other elements are kept at present-day values, as used in the PD run. The "virtual" GPI value is then subtracted from the present-day GPI value. In the case of a large difference, the assigned GPI element is considered an influential factor in terms of GPI change. Figure 10 shows the various GPIs in which individual factors are varied. Here, the logarithm of each GPI is considered because summation of the logarithm changes in virtual GPIs (Figs. 10b–f) is equivalent to the total change in logarithm GPI between the present and future [Fig. 10a; equivalent to the fractional change used in Vecchi and Soden (2007c)].

Figure 11 also shows selected area means of future change in GPI and virtual GPIs for July–October and

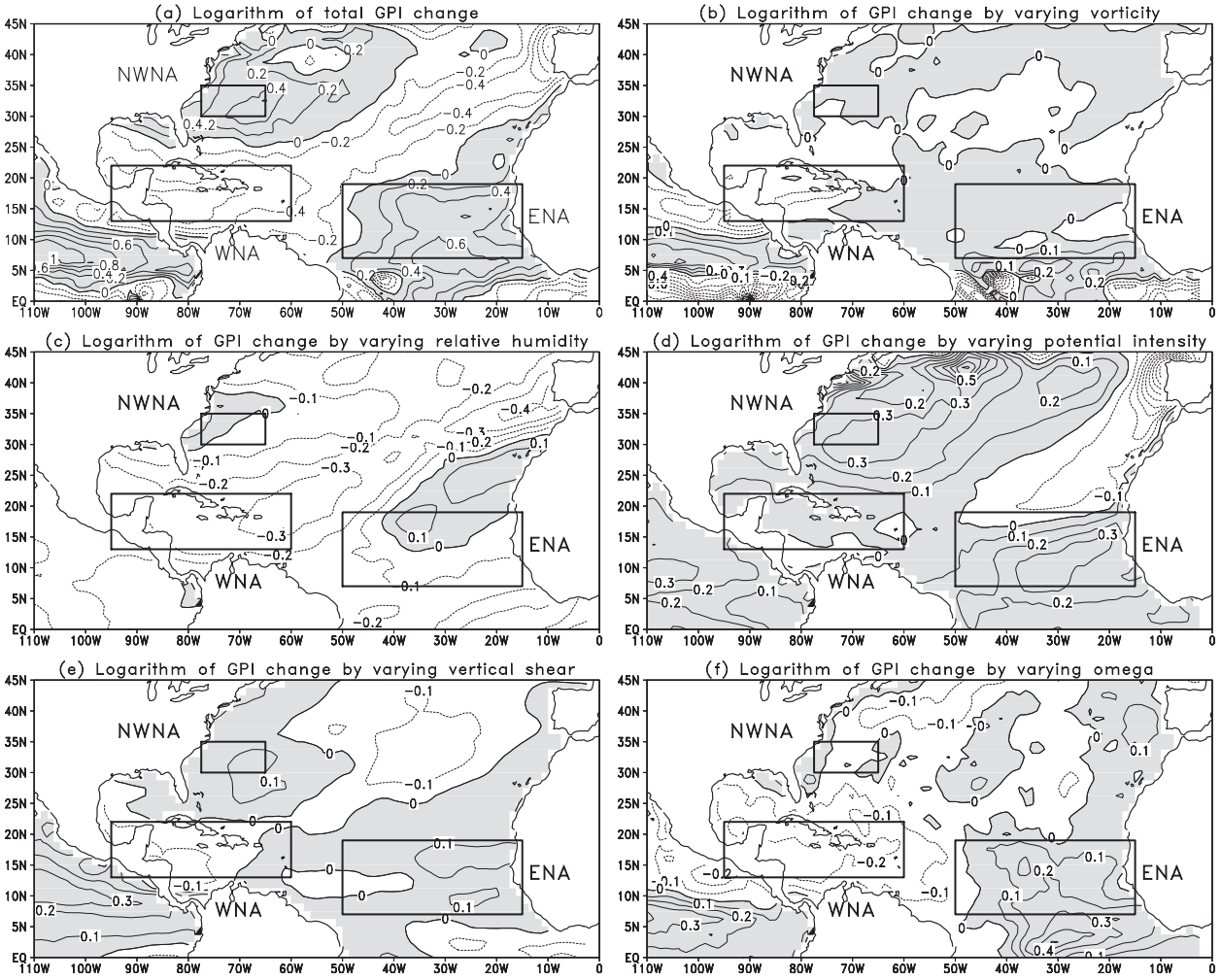

FIG. 10. Future change in GPI during JASO over the NA for (a) nonvarying GPI (i.e., difference in GPI between the GW and PD runs), and for GPI changes obtained by varying (b) vorticity, (c) relative humidity, (d) maximum potential intensity, (e) vertical shear, and (f) omega, where in each case the other variables were those of the PD run. Gray shading indicates positive values. Rectangles show ENA, WNA, and NWNA with pronounced changes in TC genesis (see text).

each month. It is notable that changes in the maximum potential intensity and omega terms make a dominant contribution to the increase in GPI within the ENA (Fig. 11b). The vertical shear term also contributes to the future increase in GPI to some degree, but the vorticity term makes only a minor contribution in the ENA (Fig. 11b). In contrast to the ENA, the relative humidity and omega terms make the largest contribution to the decrease in GPI within the WNA (Fig. 11a). The dominant contributions of these terms are robust for the entire peak season (Fig. 11a). The increase in GPI in the NWNA is due to an increase in maximum potential intensity (Figs. 10d and 11c) and in part to an increase in the vertical shear term (Figs. 10c and 11c).

Although many studies have reported that vertical shear is crucial for future change in TC genesis over the WNA (e.g., Knutson et al. 2008; Vecchi and Soden 2007c), the GPI analysis performed in the present study reveals that vertical shear has relatively small influence on the future change in GPI in the WNA. However, this does not necessarily mean that signals of circulation change projected by our simulations are markedly different from those reported in other studies. For example, the spatial distribution of future change in the vertical shear of horizontal wind (Fig. 12) is somewhat similar to that reported by Vecchi and Soden (2007c, their Fig. 1b), indicating that the vertical shear also contributes, at least to some extent, to future change in TC genesis in our projections. Vecchi and Soden (2007b) also examined the response of tropical atmospheric circulation to global warming experiments using projections by the IPCC AR4 models. The authors reported that in all models, the strength of

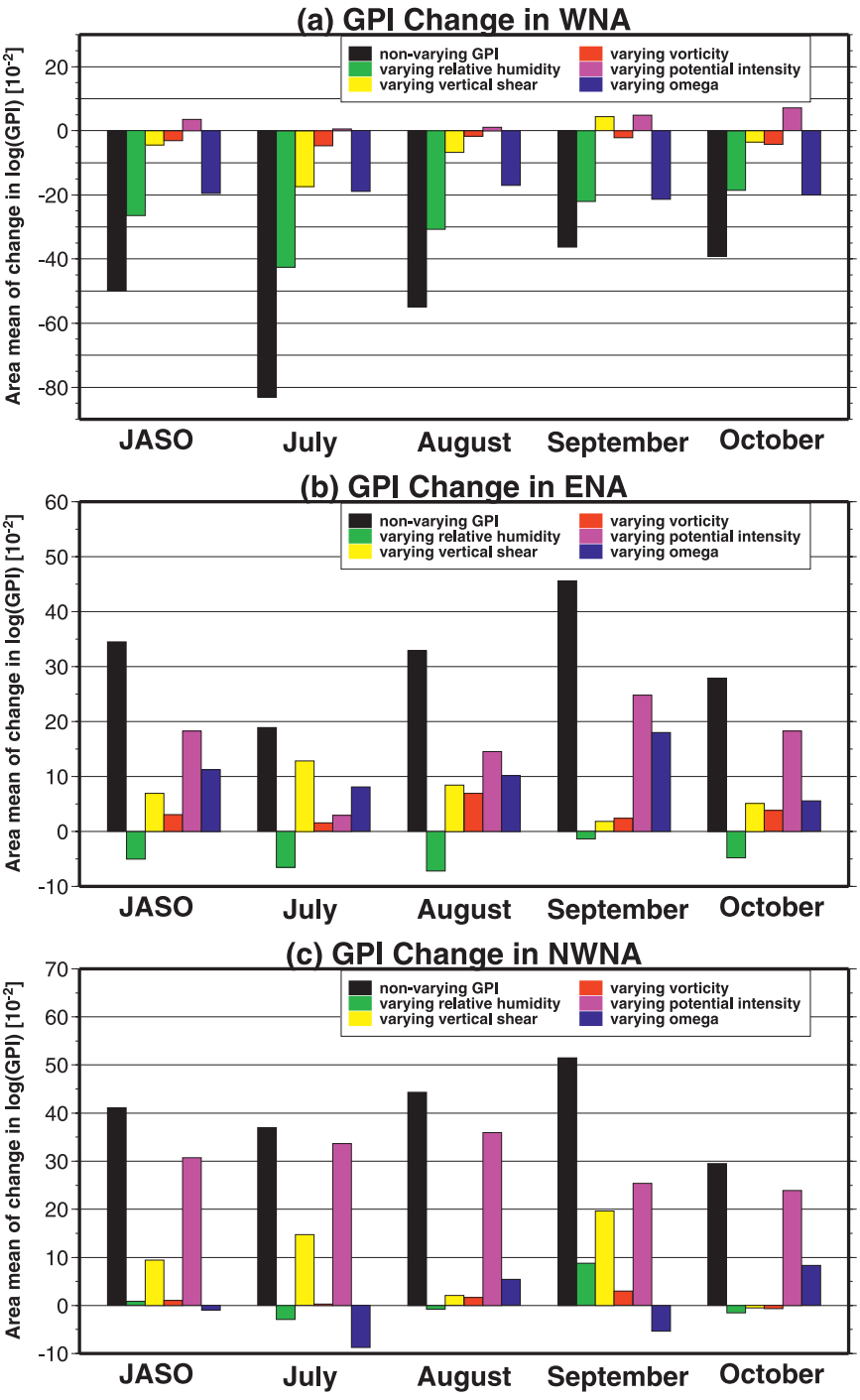

FIG. 11. Area mean of future change in the GPI during JASO and each month for (a) WNA, (b) ENA, and (c) NWNA. The nonvarying GPI (i.e., difference in GPI between the GW and PD runs; black) is the summation of GPI changes obtained by varying relative humidity (green), vertical shear (yellow), vorticity (red), maximum potential intensity (pink), and omega (blue), where in each case the other variables were those of the PD run.

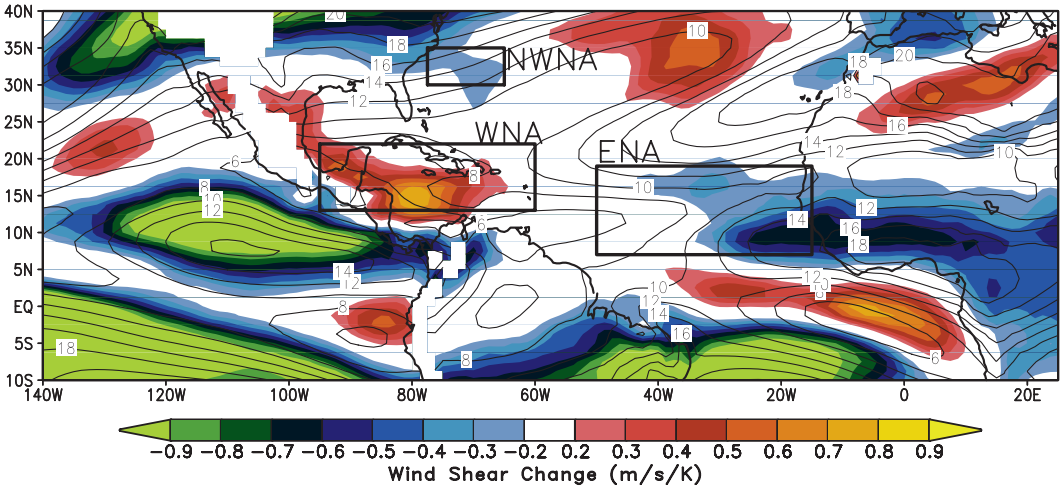

FIG. 12. Simulated change in JASO 850–200-hPa vertical wind shear (shaded; m s^{-1} $°C^{-1}$ warming). Contours show the absolute value of the vertical wind shear (m s^{-1}) simulated by the PD run. The figure corresponds to Fig. 1a of Vecchi and Soden (2007c). Rectangles show ENA, WNA, and NWNA with pronounced changes in TC genesis (see text).

atmospheric overturning circulation decreases as the climate warms. Similarly, our projection resulted in a consistent future change: a weakening in overturning circulation of about 10%–12% in the GW run. Vecchi and Soden (2007b) also reported that the weakening occurs preferentially in the zonally asymmetric (i.e., Walker) rather than zonal-mean (i.e., Hadley) component of the tropical circulation. This change is also found in our projections, whereby, weakening was more pronounced in the zonally asymmetric component than in the zonally symmetric component.

As shown above, the GPI change in the ENA is mainly due to change in large-scale vertical motion and maximum potential intensity, which appear to be related to enhanced convective activity in the ITCZ. Figure 13 shows changes in the July–October mean vertical velocity at 500 hPa and relative humidity at 600 hPa in the NA. It is clear that upward motions are enhanced in the ENA, as is relative humidity. These changes are consistent with a predicted increase in precipitation (Fig. 14). Overall, these favorable environmental conditions for convective activity promote TC genesis near the eastern Atlantic ITCZ. In contrast to the findings for ENA, the WNA features a decrease in upward motion (Fig. 13c), and reduced relative humidity (Fig. 13f) and precipitation (Fig. 14c).

The increase in convective activity in the ENA appears to be related to the prescribed future SST distribution. Figure 15 shows the distribution of forced SST and the difference between present and future values. The magnitude of increase in SST over the NA ranges from 1.8 to 2.8 K; however, the SST changes are spatially variable, with a relatively large increase in the ENA and NWNA, and a relatively small increase in the WNA. Note that precipitation is reduced in the WNA (Fig. 14c) despite the local increase in SST (Fig. 15c). This finding indicates that the increase in vertical motion in the eastern MDR region acts to enhance zonal circulation, which in turn results in the suppression of convective activity over the WNA. The enhanced Pacific ITCZ precipitation along 5°–10°N (Figs. 13c and 14c) can also reduce the ascent over the Caribbean Sea. In other words, the distribution of the SST anomaly is important not only for local TC genesis, but also for remote TC genesis in the NA.

The projected future change in NA SST is a robust signal. Figure 16 shows future change in SST relative to the tropical mean for 18 individual CMIP3 models. These models are used for computing the prescribed SST change and trend in the GW run. It is notable that most of the CMIP3 models show a larger SST increase in the ENA than in the WNA, indicating that the east–west contrast in SST change is robust across the models. Our model shows a higher frequency of TC genesis in the ENA, resulting in an increased TC number at the basin scale and increased TC frequency in the ENA. Although modeling studies have reported conflicting results regarding the future TC number, an eastward shift of frequency of TC occurrence is probably robust if a model is forced by a prescribed SST change with an east–west contrast in the tropical NA. For example, Knutson et al. (2008) used a similar pattern of SST increase in a future simulation (see their Fig. S2a) and obtained a decreased in the number of TC tracks in the WNA and an increase in the ENA (see their Fig. 2). Interestingly, Vecchi and Knutson (2008) reconstructed an observational TC dataset

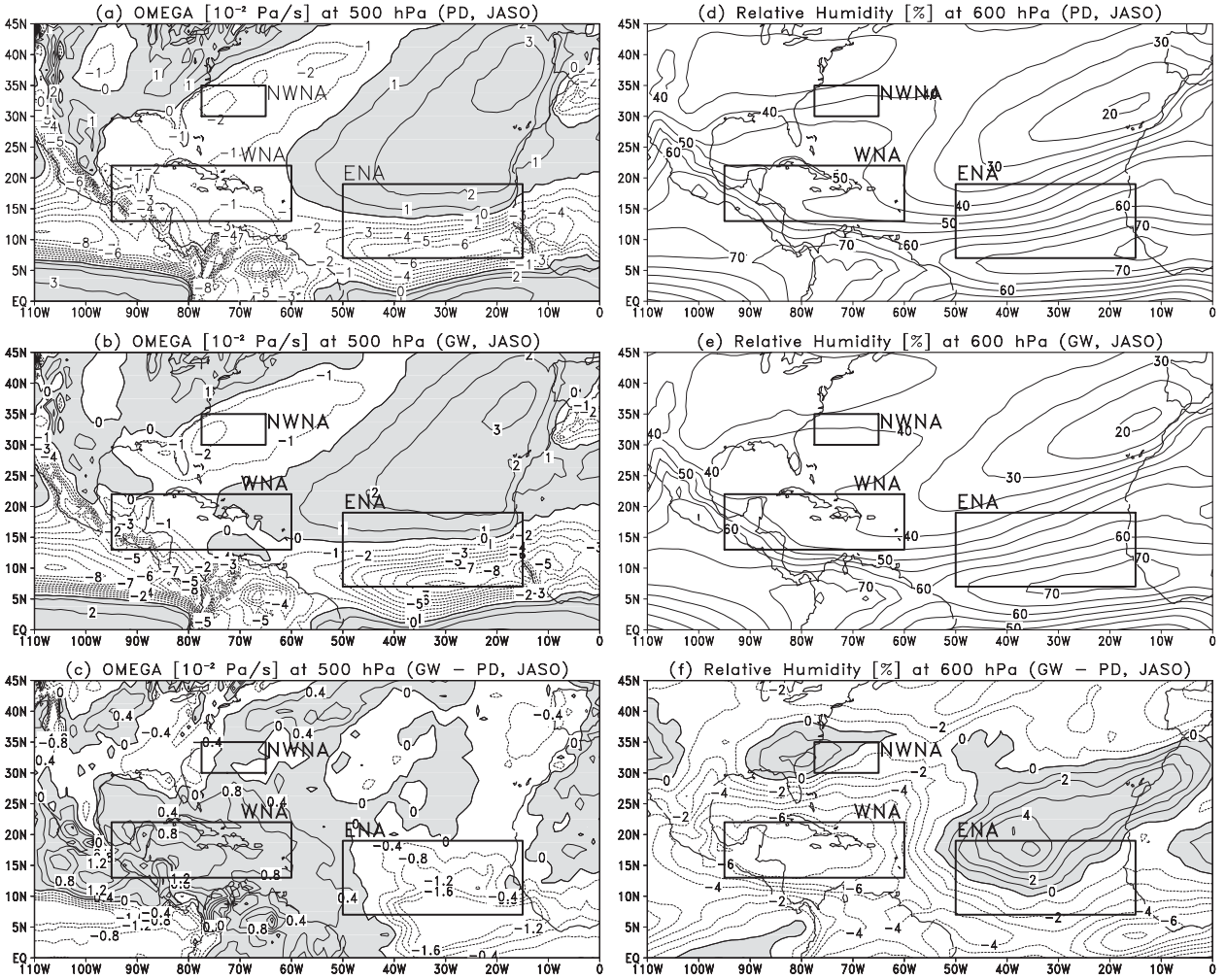

FIG. 13. (a)–(c) Vertical velocity at 500 hPa and (d)–(f) relative humidity at 600 hPa for the peak cyclone season of JASO for (a),(d) the PD run, (b),(e) the GW run, and (c),(f) the difference between the GW and PD runs. Gray shading in (a)–(c) and (f) indicates positive values. Rectangles show ENA, WNA, and NWNA regions with pronounced changes in TC genesis (see text).

since the late 1800s, and showed a similar trend with an east–west contrast in TC occurrence pattern. This consistency among different studies indicates the likelihood that a signal of climate change induced by global warming might have already appeared.

7. Summary

We conducted a pair of 25-yr climate simulations for the present day (1979–2003; PD) and the last quarter of the twenty-first century (2075–2099; GW), based on the A1B scenario using a MRI/JMA 20-km-mesh high-resolution atmospheric general circulation model (MRI/JMA-AGCM). The analysis focused on tropical cyclone (TC) activity, especially TC tracks, over the NA. The PD simulation demonstrates that the MRI/JMA-AGCM simulated a reasonably realistic climatology and variations in TC activity over the NA (Fig. 3). The observed spatial distribution of the frequency of TC occurrence during July–October (JASO) was largely captured by the PD simulation, although overestimating TC frequency in tropical regions south of 25°N and underestimating the frequency north of 25°N. The underestimation is mainly due to a lack of cyclogenesis in midlatitude regions. The correlation coefficient in interannual variation of the TC frequency between observations and the PD run was 0.46, which is statistically significant at the 95% level (Fig. 4). The simulated seasonal variation in TC counts is also realistic, although the TC genesis number is slightly underestimated for the entire year.

To better understand climate control of TC genesis, the original GPI produced by Emanuel and Nolan (2004) was modified by incorporating variations in environmental vertical motion. Overall, the modified GPI showed an

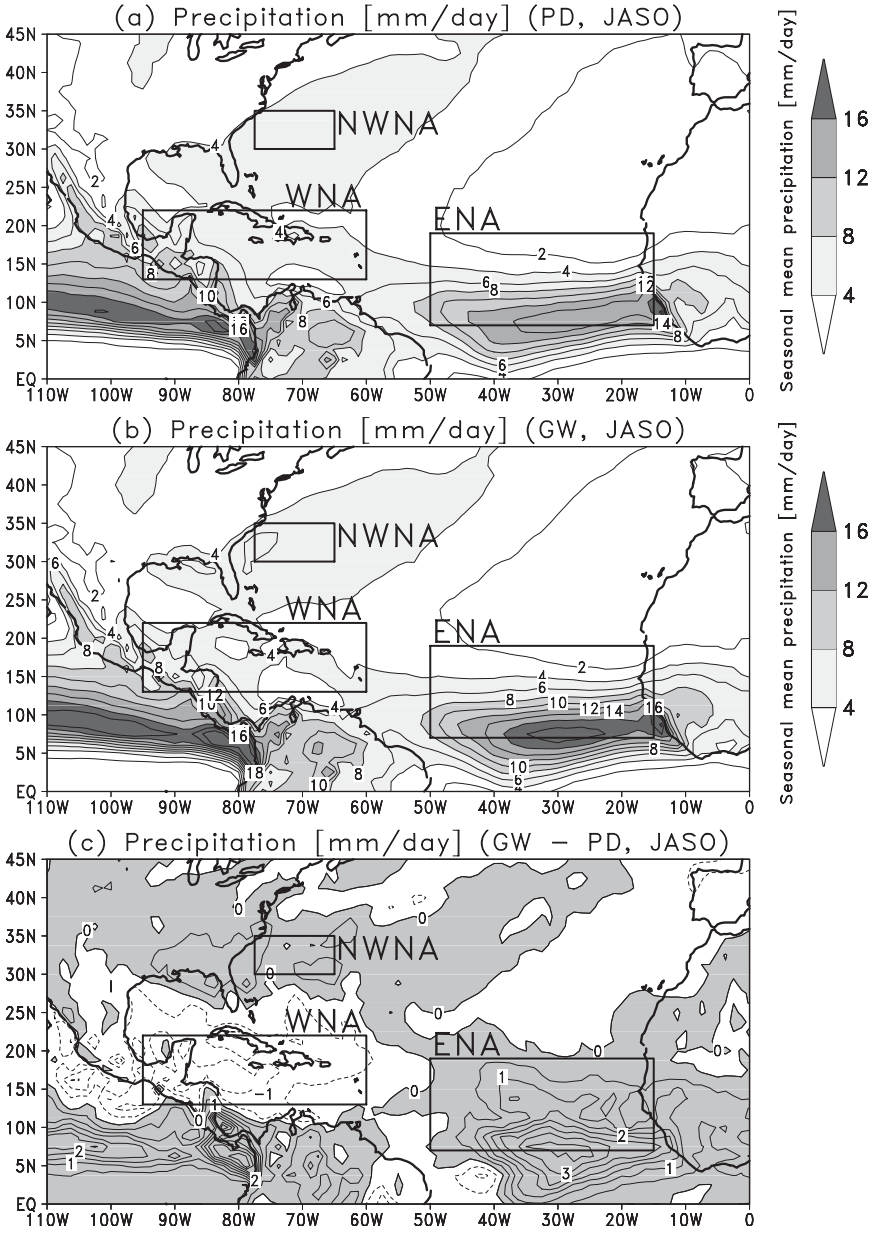

FIG. 14. Seasonal mean precipitation (mm day^{-1}) for the peak cyclone season of JASO for (a) the PD, (b) the GW run, and (c) the difference between the GW and PD runs. Gray shading in (c) indicates positive values. Rectangles show regions ENA, WNA, and NWNA with pronounced changes in TC genesis (see text).

improved representation of TC genesis climatology over the NA (Fig. 2). However, the modified GPI is still inconsistent with the observed TC genesis around the Florida peninsula.

Concerning future change, the basinwide TC frequency shows a slight increase in the GW run, but the increase was not statistically significant. The change in frequency of TC occurrence was spatially inhomogeneous, with a marked decrease in the WNA, including the Gulf of Mexico and Caribbean Sea, and an increase in the ENA and NWNA (Fig. 6). In theory, there are two possible explanations of the predicted changes in frequency of TC occurrence: changes in large-scale steering flow patterns and changes in TC genesis locations. A comparison of steering flow between the PD and GW runs reveals no significant change (Fig. 7). Furthermore, mean TC translation vectors are similar between the two runs (Fig. 8). On the other hand, we found a significant change in the

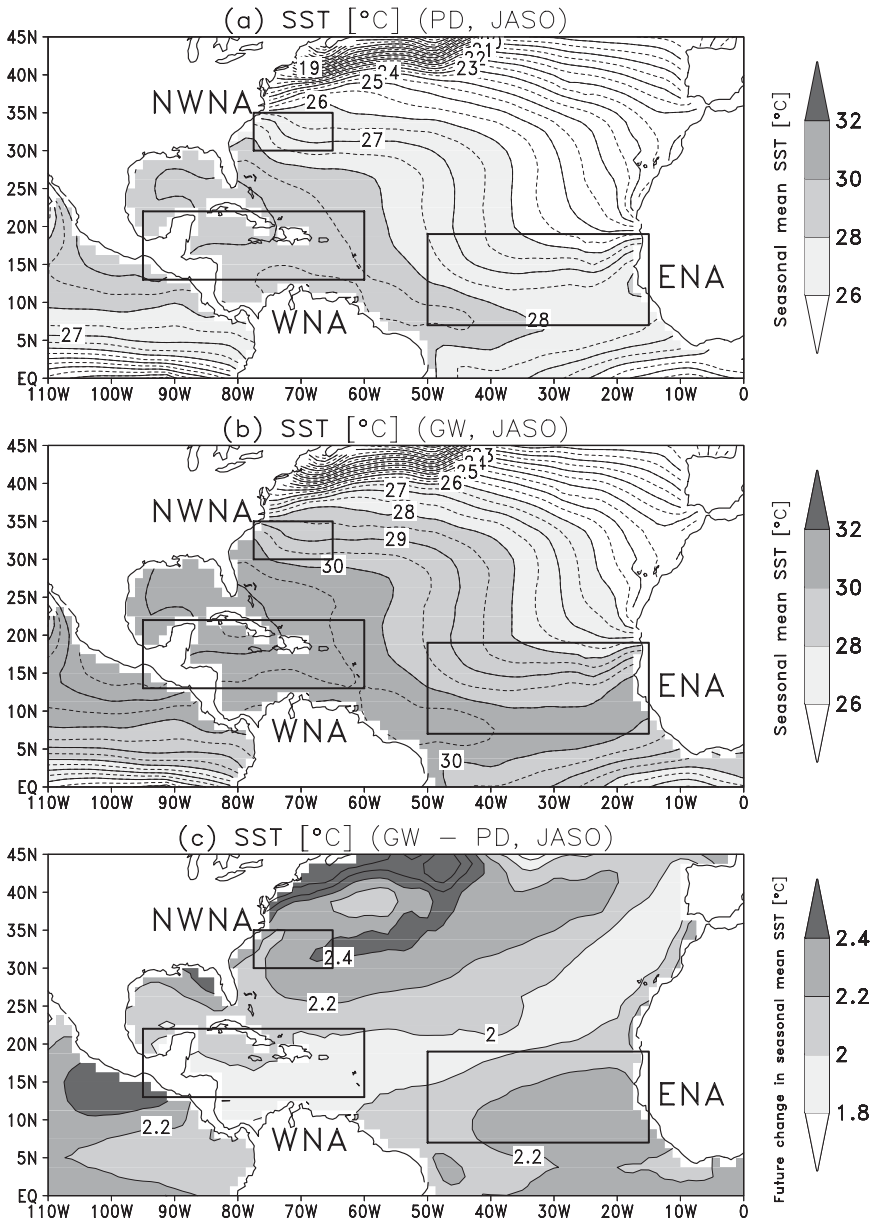

FIG. 15. Seasonal mean of prescribed SST (°C) for the peak cyclone season of JASO for (a) the PD run, (b) the GW run, and (c) the difference between the GW and PD runs. Rectangles show regions ENA, WNA, and NWNA with pronounced changes in TC genesis (see text).

locations of TC genesis between the PD and GW runs (Fig. 9), which is the major reason for the predicted future change in frequency of TC occurrence.

The signal of shift in TC locations is well captured by the projected GPI change (Fig. 9). Therefore, the GPI can be used to determine the main environmental factors responsible for future change in TC genesis. The main factors contributing to the predicted future increase in TC genesis in the ENA were changes in maximum potential intensity and vertical motion, which are related to the enhanced convective activity in the eastern Atlantic ITCZ (Fig. 11). The factors responsible for the increase in TC genesis in the NWNA were maximum potential intensity and reduced vertical shear. The former appears to be related to a relatively large local increase in SST compared with other regions in the NA, whereas the latter seems to be due to decreased westerly wind in the middle troposphere, which is a similar to a signal during El Niño years to that reported by Vecchi and Soden (2007b). The decrease in TC genesis in the WNA was mainly related to decreases in relative humidity and ascending motion. Although the prescribed sea surface

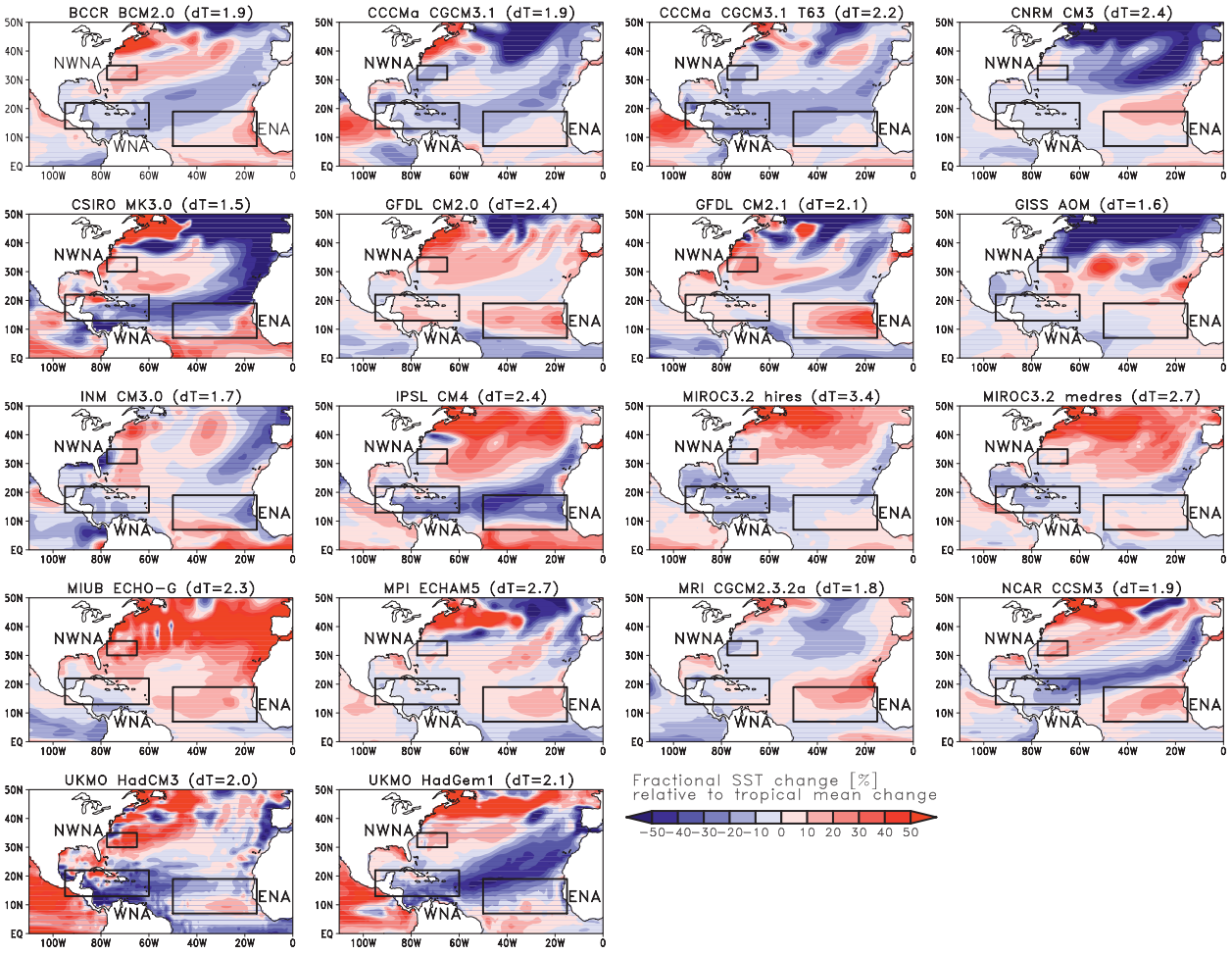

FIG. 16. Seasonal mean of SST fractional change predicted by each CMIP3 model for the peak cyclone season of JASO. The distribution of fractional SST change (%) is shown by subtracting the tropical global (20°N–20°S) averaged SST increase (°C; indicated in parentheses next to the model name). Rectangles show ENA, WNA, and NWNA with pronounced changes in TC genesis (see text).

temperature (SST) showed an increase in the WNA, convective activity decreased, indicating that the effect of remote dynamical forcing exceeds the effect of local thermodynamical forcing. In other words, the increase in convective activity in the ENA or in the eastern Pacific was sufficiently large to result in a subsidence anomaly over the WNA, which suppressed convective activity and lead to decreased TC genesis.

Overall, our experiment results suggest that the spatial pattern of the frequency of TC occurrence will show marked changes in the future, including a decrease in TC activity in the WNA and increases in the ENA and NWNA. However, we must also consider the fact that these changes are affected by marked model biases. To achieve more reliable future projections, these biases should be minimized. In addition, TC genesis appears to be sensitive to the spatial distribution of SST anomalies, and models with different physics probably respond differently to the SST increase. Although many CMIP3 models show a consistent spatial pattern of SST future change, it would be necessary to perform experiments with various spatial patterns of SST anomalies and model physics in order to reduce the degree of uncertainty in future projections.

Acknowledgments. This work was conducted under the framework of the "Projection of the Change in Future Weather Extremes Using Super-High-Resolution Atmospheric Models" project supported by the KAKUSHIN program of the Ministry of Education, Culture, Sports, Science, and Technology (MEXT) of Japan. HM would like to thank IPRC for supporting his visit. BW acknowledges support from NASA Award NNX09AG97G. The calculations were performed on the Earth Simulator. HM thanks Dr. Tim Li for his kind suggestions regarding improvements to the GPI.

REFERENCES

Anthes, R. A., R. W. Corell, G. Holland, J. W. Hurrel, M. C. MacCracken, and K. E. Trenberth, 2006: Hurricanes and global warming—Potential linkages and consequences. *Bull. Amer. Meteor. Soc.,* **87,** 623–628.

Bell, G. D., and M. Chelliah, 2006: Leading tropical modes associated with interannual and multidecadal fluctuations in North Atlantic hurricane activity. *J. Climate,* **19,** 590–612.

Bengtsson, L., M. Botzet, and M. Esch, 1996: Will greenhouse gas-induced warming over the next 50 years lead to higher frequency and greater intensity of hurricanes? *Tellus,* **48A,** 57–73.

——, K. I. Hodges, M. Esch, N. Keenlyside, L. Kornblueh, J.-J. Luo, and T. Yamagata, 2007: How may tropical cyclones change in a warmer climate? *Tellus,* **59A,** 539–561.

Bister, M., and K. A. Emanuel, 1998: Dissipative heating and hurricane intensity. *Meteor. Atmos. Phys.,* **52,** 233–240.

Broccoli, A. K., and S. Manabe, 1990: Can existing climate models be used to study anthropogenic changes in tropical cyclone climate? *Geophys. Res. Lett.,* **17,** 1917–1920.

Camargo, S. J., and A. H. Sobel, 2005: Western North Pacific tropical cyclone intensity and ENSO. *J. Climate,* **18,** 2996–3006.

——, K. A. Emanuel, and A. H. Sobel, 2007a: Use of a genesis potential index to diagnose ENSO effects on tropical cyclone genesis. *J. Climate,* **20,** 4819–4834.

——, A. H. Sobel, A. G. Barnston, and K. A. Emanuel, 2007b: Tropical cyclone genesis potential index in climate models. *Tellus,* **59A,** 428–443.

Chauvin, F., J.-F. Royer, and M. Déqué, 2006: Response of hurricane-type vortices to global warming as simulated by ARPEGE-Climat at high resolution. *Climate Dyn.,* **27,** 377–399.

Emanuel, K. A., 1995: Sensitivity of tropical cyclones to surface exchange coefficients and a revised steady-state model incorporating eye dynamics. *J. Atmos. Sci.,* **52,** 3969–3976.

——, 2005: Increasing destructiveness of tropical cyclones over the past 30 years. *Nature,* **436,** 686–688.

——, 2006: Climate and tropical cyclone activity: A new model downscaling approach. *J. Climate,* **19,** 4797–4802.

——, and D. S. Nolan, 2004: Tropical cyclone activity and global climate. Preprints, *26th Conf. on Hurricanes and Tropical Meteorology,* Miami, FL, Amer. Meteor. Soc., 240–241.

——, R. Sundararajan, and J. Williams, 2008: Hurricanes and global warming: Results from downscaling IPCC AR4 simulations. *Bull. Amer. Meteor. Soc.,* **89,** 347–367.

Goldenberg, B., C. W. Landsea, A. M. Mestas-Nuñez, and W. M. Gray, 2001: The recent increase in Atlantic hurricane activity: Causes and implications. *Science,* **293,** 474–479.

Gray, W. M., 1979: Hurricanes: Their formation, structure and likely role in the tropical circulation. *Meteorology over the Tropical Oceans,* D. B. Shaw, Ed., Royal Meteorological Society, 155–218.

——, 1984: Atlantic seasonal hurricane frequency. Part I: El Niño and 30-mb quasibiennial oscillation influences. *Mon. Wea. Rev.,* **112,** 1649–1668.

Gualdi, S., E. Scoccimarro, and A. Navarra, 2008: Changes in tropical cyclone activity due to global warming: Results from a high-resolution coupled general circulation model. *J. Climate,* **21,** 5204–5228.

Haarsma, R. J., F. F. B. Mitchell, and C. A. Senior, 1993: Tropical disturbances in a GCM. *Climate Dyn.,* **8,** 247–257.

Hatsushika, H., J. Tsutsui, M. Fiorino, and K. Onogi, 2006: Impact of wind profile retrievals on the analysis of tropical cyclones in the JRA-25 reanalysis. *J. Meteor. Soc. Japan,* **84,** 891–905.

Holland, G. J., Ed., 1993: Tropical cyclone motion. Global Guide to Tropical Cyclone Forecasting, World Meteorological Organization Tech. Doc. WMO/TD 560, Tropical Cyclone Programme Rep. TCP-31, 337 pp.

——, and P. J. Webster, 2007: Heightened tropical cyclone activity in the North Atlantic: Natural variability or climate trend? *Philos. Trans. Roy. Soc.,* **365A,** 2695–2716.

Hoyos, C. D., P. A. Agudelo, P. J. Webster, and J. Acurry, 2006: Deconvolution of the factors contributing to the increase in global hurricane intensity. *Science,* **312,** 94–97.

IPCC, 2007: *Climate Change 2007: The Physical Science Basis*. S. Solomon et al., Eds., Cambridge University Press, 996 pp.

Iwasaki, T., S. Yamada, and K. Tada, 1989: A parameterization scheme of orographic gravity wave drag with two different vertical partitionings, part I: Impacts on medium-range forecasts. *J. Meteor. Soc. Japan,* **67,** 11–27.

JMA, 2007: Outline of the operational numerical weather prediction at the Japan Meteorological Agency (appendix to WMO numerical weather prediction progress report). JMA, 194 pp. [Available online at http://www.jma.go.jp/jma/jma-eng/jma-center/nwp/outline-nwp/index.htm].

Knutson, T. R., and R. E. Tuleya, 1999: Increased hurricane intensities with CO_2-induced warming as simulated using the GFDL hurricane prediction system. *Climate Dyn.,* **15,** 503–519.

——, and ——, 2004: Impact of CO_2-induced warming on simulated hurricane intensity and precipitation: Sensitivity to the choice of climate model and convective parameterization. *J. Climate,* **17,** 3477–3495.

——, ——, and Y. Kurihara, 1998: Simulated increase of hurricane intensities in a CO_2-warmed climate. *Science,* **279,** 1018–1020.

——, J. J. Sirutis, S. T. Garner, G. A. Vecchi, and I. M. Held, 2008: Simulated reduction in Atlantic hurricane frequency under twenty-first-century warming condition. *Nat. Geosci.,* **1,** 359–364.

Krishnamurti, T. N., R. Correa-Torres, M. Latif, and G. Daughenbaugh, 1998: The impact of current and possibly future sea surface temperature anomalies on the frequency of Atlantic hurricanes. *Tellus,* **50A,** 186–210.

Kusunoki, S., J. Yoshimura, H. Yoshimura, A. Noda, K. Oouchi, and R. Mizuta, 2006: Change of Baiu rain band in global warming projection by an atmospheric general circulation model with a 20-km grid size. *J. Meteor. Soc. Japan,* **84,** 581–611.

Landsea, C. W., 2007: Counting Atlantic tropical cyclones back to 1900. *Eos, Trans. Amer. Geophys. Union,* **88,** doi:10.1029/2007EO180001.

——, B. A. Harper, K. Hoarau, and J. A. Knaff, 2006: Can we detect trends in extreme tropical cyclones? *Science,* **313,** 452–454.

LaRow, T. E., Y.-K. Lim, D. W. Shin, E. P. Chassignet, and S. Cocke, 2008: Atlantic basin seasonal hurricane simulations. *J. Climate,* **21,** 3191–3206.

Mann, M. E., and K. A. Emanuel, 2006: Atlantic hurricane trends linked to climate change. *Eos, Trans. Amer. Geophys. Union,* **87,** doi:10.1029/2006EO240001.

——, ——, G. J. Holland, and P. J. Webster, 2007a: Atlantic tropical cyclones revisited. *Eos, Trans. Amer. Geophys. Union,* **88,** doi:10.1029/2007EO360002.

——, T. A. Sabbatelli, and U. Neu, 2007b: Evidence for a modest undercount bias in early historical Atlantic tropical cyclone counts. *Geophys. Res. Lett.,* **34,** L22707, doi:10.1029/2007GL031781.

McDonald, R. E., D. G. Bleaken, D. R. Cresswell, V. D. Pope, and C. A. Senior, 2005: Tropical storms: Representation and diagnosis in climate models and the impacts of climate change. *Climate Dyn.,* **25,** 19–36.

Meehl, G. A., C. Covey, T. Delworth, M. Latif, B. McAvaney, J. F. B. Mitchell, R. J. Stouffer, and K. E. Taylor, 2007: The

WCRP CMIP3 multimodel dataset: A new era in climate change research. *Bull. Amer. Meteor. Soc.,* **88,** 1383–1394.

Mellor, G. L., and T. Yamada, 1974: A hierarchy of turbulence closure models for planetary boundary layers. *J. Atmos. Sci.,* **31,** 1791–1806.

Mizuta, R., and Coauthors, 2006: 20-km-mesh global climate simulations using JMA-GSM model–mean climate states. *J. Meteor. Soc. Japan,* **84,** 165–185.

——, Y. Adachi, S. Yukimoto, and S. Kusunoki, 2008: Estimation of the future distribution of sea surface temperature and sea ice using the CMIP3 multi-model ensemble mean. MRI Tech. Rep. 56, 28 pp. [Available at http://www.mrijma.go.jp/Publish/Technical/DATA/VOL_56/56.html.]

Murakami, H., and T. Matsumura, 2007: Development of an effective non-linear normal mode initialization method for a high resolution global model. *J. Meteor. Soc. Japan,* **85,** 187–208.

——, ——, R. Sakai, A. Noda, and S. Kusunoki, 2008: Verification typhoon forecasts for a 20-km-mesh high-resolution global model. *J. Meteor. Soc. Japan,* **86,** 669–698.

Nguyen, K.-C., and K. J. E. Walsh, 2001: Interannual, decadal, and transient greenhouse simulation of tropical cyclone-like vortices in a regional climate model of the South Pacific. *J. Climate,* **14,** 3043–3054.

Onogi, K., and Coauthors, 2007: The JRA-25 reanalysis. *J. Meteor. Soc. Japan,* **85,** 369–432.

Oouchi, K., J. Yoshimura, H. Yoshimura, R. Mizuta, S. Kusunoki, and A. Noda, 2006: Tropical cyclone climatology in a global-warming climate as simulated in a 20-km-mesh global atmospheric model: Frequency and wind intensity analysis. *J. Meteor. Soc. Japan,* **84,** 259–276.

Peterson, T. C., and Coauthors, 2008: Why weather and climate extremes matter. Weather and Climate Extremes in a Changing Climate, National Climatic Data Center. [Available online at http://www.climatescience.gov/Library/sap/sap3-3/final-report/default.htm.]

Pielke, R. A., C. Landsea, M. Mayfield, J. Laver, and R. Pasch, 2005: Hurricanes and global warming. *Bull. Amer. Meteor. Soc.,* **86,** 1571–1575.

Randall, D., and D.-M. Pan, 1993: Implementation of the Arakawa-Schubert cumulus parameterization with a prognostic closure. *The Representation of Cumulus Convection in Numerical Models, Meteor. Monogr.,* No. 46, Amer. Meteor. Soc, 137–144.

Rayner, N. A., D. E. Parker, E. B. Horton, C. K. Folland, L. V. Alexander, and D. P. Rowell, 2003: Global analyses of sea surface temperature, sea ice, and night marine air temperature since the late nineteenth century. *J. Geophys. Res.,* **108,** 4407, doi:10.1029/2002JD002670.

Royer, F.-J., F. Chauvin, B. Timbal, P. Araspin, and D. Grimal, 1998: A GCM study of the impact of greenhouse gas increase on the frequency of occurrence of tropical cyclones. *Climatic Change,* **38,** 307–343.

Sato, N., P. J. Sellers, D. A. Randall, E. K. Schneider, J. Shukla, J. L. Kinder, III, Y.-T. Hou, and E. Albertazzi, 1989: Effects of implementing the simple biosphere model (SiB) in a general circulation model. *J. Atmos. Sci.,* **46,** 2257–2282.

Schmidlin, T. W., 2006: On evacuation and deaths from Hurricane Katrina. *Bull. Amer. Meteor. Soc.,* **87,** 754–756.

Sellers, P. J., Y. Mintz, Y. C. Sud, and A. Delcher, 1986: A simple biosphere model (SiB) for use within general circulation models. *J. Atmos. Sci.,* **43,** 505–531.

Shibata, K., and T. Aoki, 1989: An infrared radiative scheme for the numerical models of weather and climate. *J. Geophys. Res.,* **94,** 14 923–14 943.

——, and A. Uchiyama, 1992: Accuracy of the delta-four-stream approximation in inhomogeneous scattering atmospheres. *J. Meteor. Soc. Japan,* **70,** 1097–1109.

Smith, R. N. B., 1990: A scheme for predicting layer clouds and their water content in a general circulation model. *Quart. J. Roy. Meteor. Soc.,* **116,** 435–460.

Stowasser, M., Y. Wang, and K. Hamilton, 2007: Tropical cyclone changes in the western North Pacific in a global warming scenario. *J. Climate,* **20,** 2378–2396.

Sugi, M., A. Noda, and N. Sato, 2002: Influence of the global warming on tropical cyclone climatology. *J. Meteor. Soc. Japan,* **80,** 249–272.

——, H. Murakami, and J. Yoshimura, 2009: A reduction in global tropical cyclone frequency due to global warming. *SOLA,* **5,** 164–167.

Tanaka, T. Y., K. Orito, T. Sekiyaam, K. Shibata, M. Chiba, and H. Tanaka, 2003: MASINGAR, a global tropospheric aerosol chemical transport model coupled with MRI/JMA98 GCM: model description. *Pap. Meteor. Geophys.,* **53,** 119–138.

Trenberth, K. E., and D. J. Shea, 2006: Atlantic hurricanes and natural variability in 2005. *Geophys. Res. Lett.,* **33,** L12704, doi:10.1029/2006GL026894.

Tsutsui, J., 2002: Implications of anthropogenic climate change for tropical cyclone activity. *J. Meteor. Soc. Japan,* **80,** 45–65.

Unisys, cited 2009: Unisys weather hurricane tropical data. [Available online at http://weather.unisys.com/hurricane/.]

Vecchi, G. A., and B. J. Soden, 2007a: Effect of remote sea surface temperature change on tropical cyclone potential intensity. *Nature,* **450,** 1066–1070.

——, and ——, 2007b: Global warming and the weakening of the tropical circulation. *J. Climate,* **20,** 4316–4340.

——, and ——, 2007c: Increased tropical Atlantic wind shear in model projections of global warming. *Geophys. Res. Lett.,* **34,** L08702, doi:10.1029/2006GL028905.

——, and T. R. Knutson, 2008: On estimates of historical North Atlantic tropical cyclone activity. *J. Climate,* **21,** 3580–3600.

Walsh, K. J. E., K.-C. Nguyen, and J. L. McGregor, 2004: Fine-resolution regional climate model simulations of the impact of climate change on tropical cyclones near Australia. *Climate Dyn.,* **22,** 47–56.

Webster, P. J., G. J. Holland, J. A. Curry, and H.-R. Chang, 2005: Changes in tropical cyclone number, duration, and intensity in a warming environment. *Science,* **309,** 1844–1846.

Wu, L., and B. Wang, 2004: Assessing impact of global warming on tropical cyclone tracks. *J. Climate,* **17,** 1686–1698.

——, ——, and S. Geng, 2005: Growing typhoon influence on east Asia. *Geophys. Res. Lett.,* **32,** L18703, doi:10.1029/2005GL022937.

Yoshimura, H., and T. Matsumura, 2003: A semi-Lagrangian scheme conservative in the vertical direction. CAS/JSC WGNE Research Activities in Atmospheric and Oceanic Modeling 33, 319–320.

Yoshimura, J., M. Sugi, and A. Noda, 2006: Influence of greenhouse warming on tropical cyclone frequency. *J. Meteor. Soc. Japan,* **84,** 405–428.

Yukimoto, S., and Coauthors, 2006: Present-day climate and climate sensitivity in the Meteorological Research Institute Coupled GCM, Version 2.3 (MRI-CGCM2.3). *J. Meteor. Soc. Japan,* **84,** 333–363.

Zhao, M., I. M. Held, S.-J. Lin, and G. A. Vecchi, 2009: Simulations of global hurricane climatology, interannual variability, and response to global warming using a 50-km resolution GCM. *J. Climate,* **22,** 6653–6678.